Tracing the evolution of the Frisian Inlet using optical and radar satellite imagery

A remote sensing study

Mes, J.W.F.

May 7, 2020

Abstract

The Wadden Sea is a dynamic region undergoing rapid change due to natural morphodynamic processes. Monitoring these changes and extracting conceptual models is limited by the frequency of bathymetric studies (once every ∼6 years in the Netherlands). We therefore present several new techniques for studying these changes using high cadence (every ∼8 days to 2 months) and high resolution (10 - 30 m) optical and radar satellite imagery. The Frisian Inlet is used as a case study for these techniques. This region has both sub- to intertidal (channels, sandbars and shoals) and supratidal morphological features (islets and islands) which have been studied extensively in the past. The existing conceptual models for these features comprising inlet channel migration cycles and shoal growth patterns are based mainly on the existing low cadence bathymetry. They are assessed using the new techniques, resulting in both a test of existing morphodynamical theories and serving as a prime example for the application of the novel remote sensing techniques. These techniques can be applied in other parts of the Wadden Sea and in tidal flats around the globe. We also present an outlook to further possible developments of remote sensing techniques in this field.

1 Introduction

This work will cover two main aspects: morphodynamics of the Frisian Inlet and novel remote sensing techniques. With the latter we aim to improve the quality of the assessment of the former, making these topics heavily intertwined. The research objectives are discussed in Section 1.1. These are quite specific and are given context in the sections regarding the region of interest (Section 2) and the data used for the analysis (Section 3). Section 4 covers the data processing, while Section 5 discusses the results of the applied methods. Section 6 ends this report with conclusions and recommendations.

1.1 Research Objectives

When looking in detail at a complex morphodynamic system such as the Frisian Inlet many questions arise. Below we will list a series of research questions which we will address in this work and a list of ones which are outside of the current scope. Both are subdivided into questions regarding the Frisian Inlet itself and questions about the possible research methods including remote sensing.

1.1.1 Objectives of this work

The Frisian Inlet

- Has the cyclic behaviour of the Pinkegat persisted since the detailed description by Oost

(1995)?
- Is the Engelsmanplaat shoal-merging cycle still valid?
- Do the nourishments at Ameland impact the sediment bypassing at the Pinkegat?

Research Methods

- Can we use satellite data to aid in detecting morphodynamical change?
- Can we use the satellite data to detect sediment bypass?

1.1.2 Outside of the current scope

These questions arose during data exploration and processing. They will not be elaborated upon to maintain the focus of this report.

The Frisian Inlet

- What is the shape of the Holocene clay layer below the Engelsmanplaat?
- Why has the Zoutkamperlaag not migrated westward or conversely, why is the east side of the Engelsmanplaat so extremely straight (De Haan et al., 1983) and stable in its position (based on bathymetric surveys since 1927, hydrographic maps since 1810 (De Haan et al., 1983) and historic maps since the middle of the 18th century)?
- Why are there many more smaller channels in the backbarrier basin of the Pinkegat compared to the Borndiep and Zoutkamperlaag basins? In other words, why is the fractal dimension of the channels larger?

Research Methods

- Can we determine bathymetry from satellite imagery?
- Could synthetic aperture radar (SAR) interferometry be used to determine sedimentation and erosion on tidal flats on millimeter scales?
- On both optical and SAR imagery the channel banks in the backbarrier basin of the Pinkegat have a higher reflectance than other areas in the Wadden Sea. Does this indicate that more sand is present in the top layer? If so, why is there more sand in the top layer of the Pinkegat basin than in for example the Borndiep or Zoutkamperlaag basins?

2 Region of Interest

The Frisian Inlet, known in Dutch as the "Friese Zeegat" (FZG), is located between the islands of Ameland and Schiermonnikoog. It is a complex of tidal channels and shoals which is part of the Dutch Wadden Sea. This region of tidal channels and barrier islands formed $\sim$ 5500 years ago after the last Ice Age, the Wechselian, on the coastal plain of northwest Europe (Oost, 1995). Its formation was induced by a combination of sea level rise ($\sim 1\,\mathrm{cm\,yr^{-1}}$ in the early Holocene to $0 - 0.1\ \mathrm{cm\,yr^{-1}}$ after 6000 B.P.) and land subsidence ($0.10 - 0.15\ \mathrm{cm\,yr^{-1}}$), with sediments imported from rivers like the Rhine and the North Sea itself (Oost, 1995). The topography at the end of the Pleistocene dominated the subsequent evolution of the region. The Boorne, Hunze and Ems river valleys, visible in Figure 1(a) as three indents in the coast running from west to east, became the Middelzee, Lauwerszee and Ems/Dollard estuaries or embayments in Medieval times. The imprint of these estuaries is still visible in the current Pleistocene top layer, as shown in Figure 1(b). The Frisian Inlet currently consists of two sub-inlets, the "Pinkegat" and "Zoutkamperlaag".

2.1 Zoutkamperlaag

Before its closure in 1969, the Lauwerszee was the defining morphological feature of the Frisian Inlet. In the Medieval period the estuary emptied into the Lauwers channel east of Schiermonnikoog, but in the 14th century the Zoutkamperlaag, until then a relatively minor channel west of Schiermonnikoog, broke through and also started to feed the Lauwerszee (De Haan et al., 1983; Oost, 1995; Mulder, 2015). Both channels coexisted as drainage channels of the Lauwerszee up to at least the 18th century (Mulder, 2015). This was coupled with a large eastward shift of Schiermonnnikoog to approximately its current position (3.5 km erosion at its western end and 6 km growth at its eastern end between 1300 and 1850 A.D.). Ameland, bordering the study area in the west, underwent a smaller eastward migration (1.5 km erosion at the west and 3.5 km growth in the east between 1650 and 1969 A.D.) (Oost, 1995; Sha, 1992, Fig. 4.1 & 4.2). This shift of the Frisian Inlet before its closure was most likely caused by its unfavourable position with respect to the Lauwerszee. The migration of the inlet halted when through land reclamation in the Lauwerszee the tidal basin of the Frisian Inlet shrunk (De Haan et al., 1983).

2.2 Pinkegat

The second channel system in the Frisian Inlet, the Pinkegat, rounds the eastern end of Ameland. As the tidal wave propagates from west to east along the North Sea coast, the flood enters the Ameland inlet west of the island earlier than the Pinkegat, resulting in a tidal divide markedly positioned east of the center of the island. This results in a significantly smaller tidal basin of the Pinkegat ($\sim 53\,\mathrm{km^2}$ in 1992) compared to channels rounding the western end of the islands like the Zouterkamperlaag ($\sim 126\,\mathrm{km^2}$ in 1992) (Oost and De Haas,

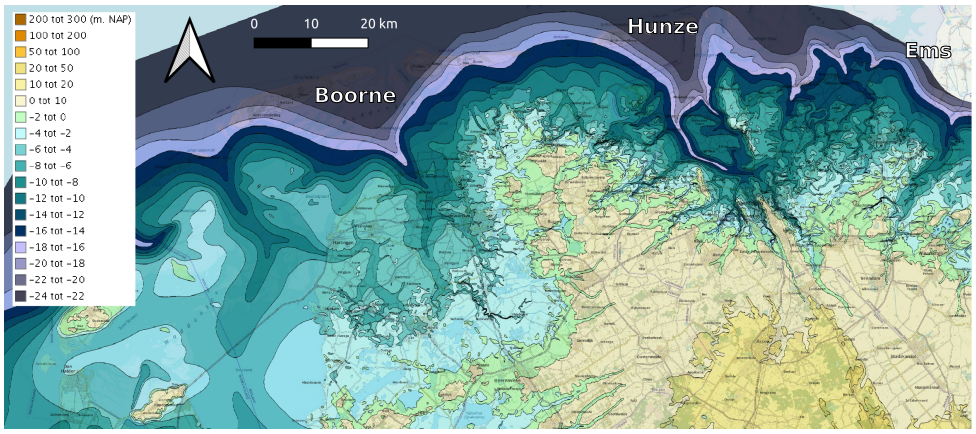

(a) 11 000 B.P.

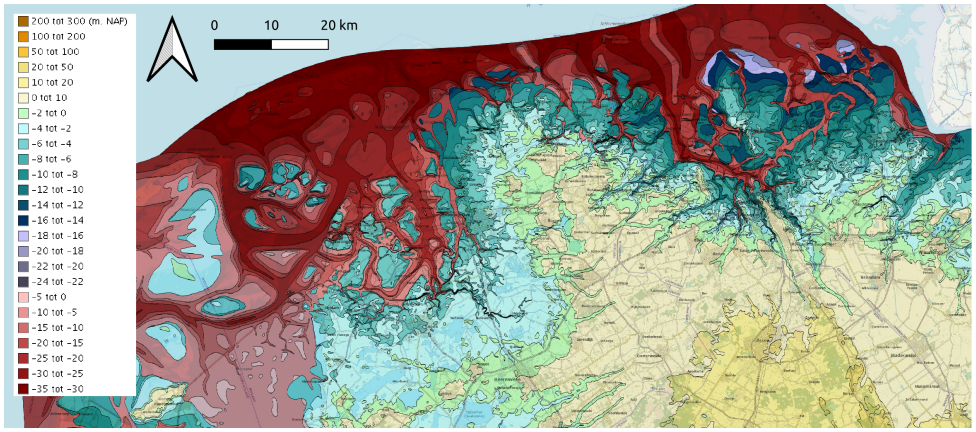

(b) Current

Figure 1: Height of the top Pleistocene layer at 11 000 B.P. and at current in meters above NAP (≈ mean sea level). For the current Pleistocene top layer height the regions with Holocene erosion caused by coastal channels are shown in red. Height map source: Rijksdienst voor het Cultureel Erfgoed/nationaalgeoregister.nl. Background map source: J.W. van Aalst, opentopo.nl. The Boorne, Hunze and Ems estuaries are annotated in Fig. 1(a).

1992; Sha, 1992), resulting in a smaller tidal prism ($\sim 100 \cdot 10^6 m^3$ versus $\sim 208 \cdot 10^6 m^3$, respectively (Sha, 1992)). The ebb-tidal deltas are also comparatively smaller: in 1992 $\sim 22\,km^2$ and $\sim 94\,km^2$ respectively. The formation of the Pinkegat was most likely due to this difference between the two basins which were up until the 15th century drained by a single channel. Around this time the Pinkegat broke through the low island head of Ameland. This also resulted in a shoal between the Pinkegat and Zoutkamperlaag channels, which is now known as the "Engelsmanplaat" (De Haan et al., 1983).

The Frisian Inlet has a tidal range of $\sim 2\,m$, placing it in the lower end of the meso-tidal range, and a mean significant wave height of $\sim 0.7\,m$, making the inlet a mixed energy, tide dominant region (Wang and Oost, 2011). Although the dominant wind direction is southwest, the dominant wave direction is northwest due to the fact that the coast is oriented east-west.

2.3 The Engelsmanplaat

The shoal Engelsmanplaat (a local alternative name is "De Kalkman") is located between the two channels of the Frisian Inlet. It has been in existence since around 1580 when it was formed together with the Pinkegat (De Haan et al., 1983). Between 1832 and 1992 the shoal eroded on its western side over a distance of 4.9 km to an east-west width of 2.2 km in 1992 (Oost, 1995), with slower erosion since 1927. In 2019, the east-west width was unchanged at 2.2 km (based on the 2019 depth sounding of the Frisian Inlet, see Section 3.1.3 for details on this data). During this period the eastern point of Ameland, known as "De Hôn", saw massive changes. The coastline at the tip of the island moved eastward by 4.3 km between 1910 and 1950, and subsequently 2.5 km westward until 1980. The largest growth was between 1930 and 1940 in the order of $\sim 300\,m\,yr^{-1}$ (Sha, 1992, Fig. 4.4). The current RD-longitude[1]

[1]The "Rijksdriehoekscoördinaten" are a set of cartesian coordinates with units of meters widely used in the Nether-

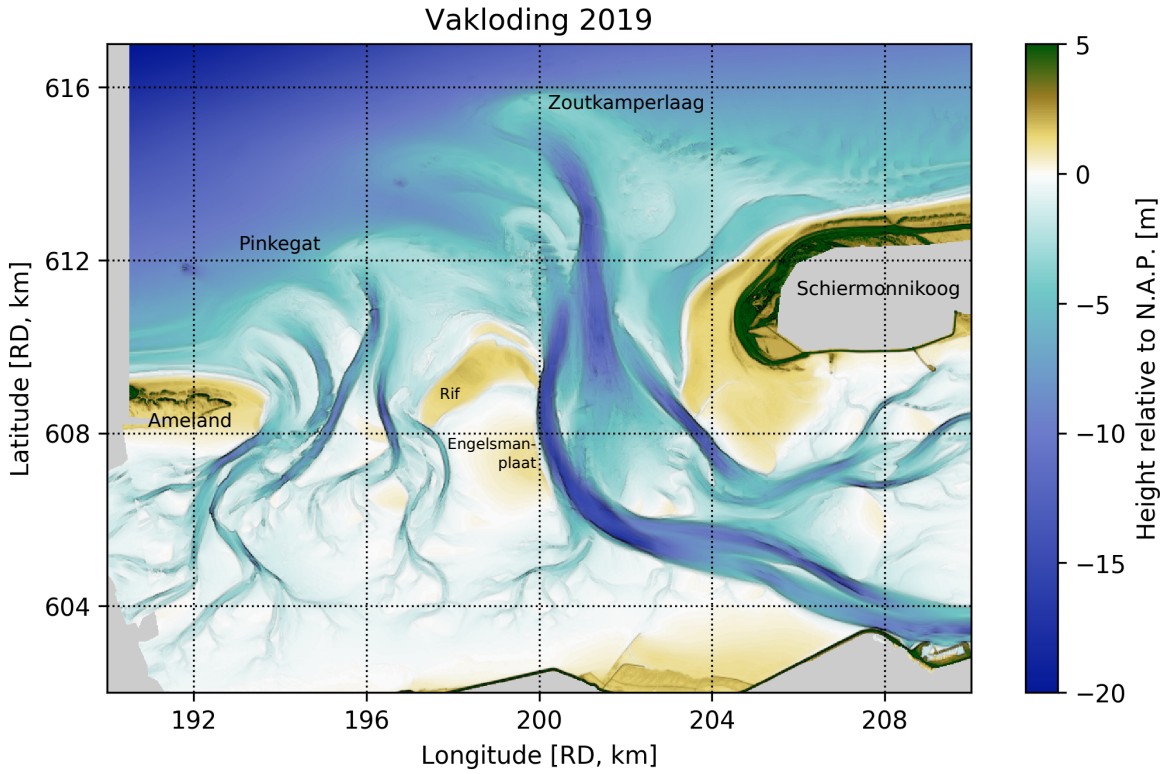

Figure 2: Vakloding of the region of interest from 2019.

coordinate of the tip of the island is 193.70 km based on the 2019 vakloding (see Figure 2). The 4.3 km eastward migration of De Hôn in the first half of the 20th century can be attributed to the shift of the Pinkegat, which allows sediments to be deposited in its inner bend. Oost (1995) partially attributes this shift of the Pinkegat to the eastward movement of the Ameland Inlet.

The east side of the Engelsmanplaat on the other hand is rather stable, seeing only a $\sim$ 250 m shift to the east remarkably straight into the outer curve of the Zoutkamperlaag. A plausible explanation is the infill of the Zoutkamperlaag due to the closure of the Lauwerszee in 1969, decreasing the tidal prism by a third from $\sim 317 \cdot 10^6$ to $\sim 208 \cdot 10^6$ m^3 (Van Sijp, 1989), resulting in a decrease of the channel cross-section (Oost, 1995) (see also Figure 5 right panel). The sediments involved in this channel infill were mostly derived from neighbouring tidal flats (Winkelmolen and Veenstra, 1974), which therefore saw significant erosion. Around 1969 the Engelsmanplaat hosted many embryonal dunes and was a nesting ground for various bird species, with a peak shoal height of 1.87 m above NAP[2] in 1967 based on the vakloding of that year (see Figure 5 left panel). An impression of the situation from the ground is shown in Figure 3(a). Many embryonal dunes with a height of ~40 cm are visible. The dunes were located in two groups: a large central core just west of the center of the islet and a smaller group in the NE corner. The northern and eastern shores were quite steep, while the southern and western sides of the shoal were low and broad, with a low slope to the intertidal flats.

In 1975 the peak height of the Engelsmanplaat had decreased to 1.0 m above NAP, resulting in flooding even at regular tidal water levels (Oost and De Haas, 1992) (see also Figure 3(b)). Erosion decreased in the second part of the 70's with the eastern section remaining stable and the western section lowering from $\sim$ 0.9 to $\sim$ 0.3 m above NAP in 1975 and 2019 respectively (see Figure 4). Around 1967 a narrow spit formed on the eastern side of the shoal which became just about supratidal ($\sim$ 1.30 m above NAP in 2019) and subsequently migrated southwards by $\sim$ 1 km. It is named the "Hiezel", after the small gully just south of it during the years that it formed. An overview of the vaklodingen of the Frisian Inlet is shown in Appendix A Figure 18.

Illustrative of the erosion the Engelsmanplaat underwent since the closure of the Lauwerszee are the archaeological findings in the area. In 1977 the foundation of a large navigational beacon, cut down at the beginning of the first world war to prevent it

lands.

[2] "Normaal Amsterdams Peil" or the Amsterdam Ordnance Datum which is rougly equal to the current mean sea level. At the inception of its predecessor the "Amsterdams Peil" (non-normalized) in 1684 it was taken as the average high tide level. Since this period, known as the "Little Ice Age", mean sea level has risen by at least 80 cm, resulting in the mean instead of high tide sea level being roughly equal to NAP.

(a) 1973 (b) 1977

Figure 3: Fig. 3(a): the Engelsmanplaat in the summer of 1973. Large embryonal dunes and wide, shell covered flats are visible in the foreground and Ameland in the background. The viewing direction is indicated in the sketch below (WSW, north is up). The photo was taken from the smaller dune complex in the NE. Fig. 3(b): the Engelsmanplaat during a flood in the summer of 1977. Weather conditions are fair, indicating a minor flood. Nesting birds and embryonal dunes are visible in the foreground. Image attribute: Ron Mes.

being useful for invading forces, was found. In 2010 through dendrochronology it was determined that it was built in 1858 (Stichting Verdronken Geschiedenis, 2010). The tops of the sawed-off wooden stilts currently reside ~ 50 cm above the surrounding tidal flat. In 2014 220 m north-east of this historic beacon a 5 m long piece of a shipwreck was found (Mulder, 2015), with the wood dated to 1749 ± 7 yr. Fitting the dynamic nature of the Wadden Sea, the wreck was covered by sand the following year. There are two other sets of old beacon foundations present in the northwest corner of the Engelsmanplaat which have not been dated yet and of which the origin is unknown (Stichting Verdronken Geschiedenis, 2010). However, their presence does indicate that this section of the Engelsmanplaat has not undergone significant change in the last several centuries.

The erosion resistant "plug" Several authors (e.g. Oost and De Haas (1992); Oost (1995)) attribute the apparent erosion resistance of the Engelsmanplaat (especially on its eastern side) to the presence of marine clay from the Holocene, as originally reported by Sha (1992, Fig. 5.1.4a with core ID 91.031). De Haan et al. (1983) already proposed the presence of this clay layer in the first edition of the booklet as an explanation of the erosion resistance of the shoal. They however reject this statement in the second edition by citing research from the Dutch Geological Survey which found no solid clay core below the Engelsmanplaat. This is in apparent contradiction with the results from Sha (1992).

Oost and De Haas (1992) and Oost (1995) cite the clay layer as having origins around 5000 - 4000

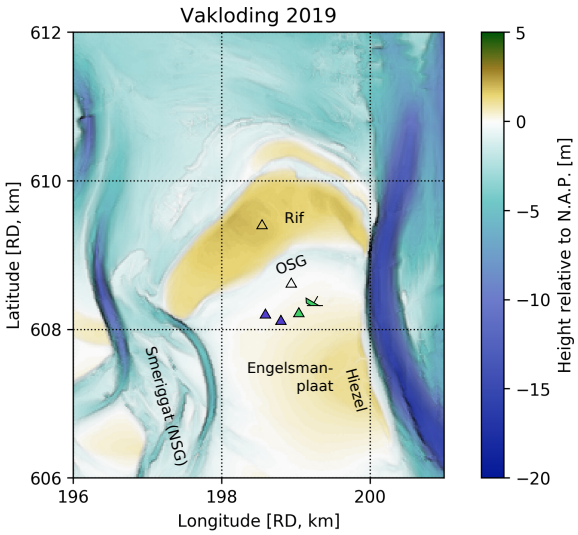

Figure 4: Vakloding of the Engelsmanplaat and Rif in 2019. Beacon remnants are indicated with triangles. The green triangle and ship icon indicate the locations of the beacon remnant and shipwreck of which the dates are known. For the beacons indicated with blue triangles, the dates are unknown. The triangles without fill are beacons which were lost or removed due to stability issues, presumably caused by the SE migration of the Smeriggat (OSG) (see also WadgidsenWeb).

B.P. and being at depths of −5 to −10 m relative to NAP. As the Zoutkamperlaag has a maximum depth near the Engelsmanplaat of roughly −18.8 m in 1967 and −14.5 m in 2019 based on the vaklodingen of these years, this stable clay layer could halt westward migration of the channel. However, this reported clay layer depth is incorrect: the actual depth of the clays in the drilling just NW of the Engelsmanplaat as indicated in Fig. 5.1.4a of Sha (1992) is between roughly −13.4 and −19.9 m relative to NAP. The digitalized core data accessible on the *DINOloket*[3] show a depth between −13.45 and −19.94 m relative to NAP. At its current depth, the Zoutkamperlaag would only be blocked by 1 m of clay at the very bottom and thus narrowest section of the channel cross-section. It therefore seems unlikely that this layer exposed by this specific drilling resists the erosive force of the channel. However, the *DINOloket* also has core data on two other drillings[4] located on the south-eastern side of the Engelsmanplaat in the channel wall itself. Both are from 1946 and indicate a clay layer starting at the channel bottom at −5 m and extending to −7.5 m NAP. The vaklodingen of 1967 and 1987 in Figure 5 both indicate a broad shelf at about −5 m depth in the channel at the positions of the drillings. The 2019 vakloding (Figure 2) has the southern drilling location covered by a mudflat, while the northern one is again located on (the edge of) a shelf of the same depth, which now shows a peculiar underwater "cliff face" feature running SSE - NNW with a vertical displacement of ∼ 7.5 m (-15 to −7.5 m NAP) over a distance of ∼ 65 m. The shelf drops off to −12.5 m NAP at the same longitude as the Engelsmanplaat. As this is roughly the same depth as the clay layer found by Sha (1992), this shelf could be this clay layer dropping from roughly −5 m depth to −13.5 m depth from south-east to just north of the Engelsmanplaat. With this theory in mind, the hypothesis of a layer of clay resisting the migration of the Zoutkamperlaag seems much more plausible.

Whether the Engelsmanplaat is necessary to maintain a double inlet configuration for the Frisian Inlet is currently still debated. Wang (1991) conclude after morphodynamical modelling of a simplified double inlet system that a central shoal or bank is necessary for the computation to provide a stable solution. However, Leeuwen (2002, on p. 123) found that in a simulated inlet of roughly the same shape and size as the Frisian Inlet with a gently sloping coastal plain two inlets naturally form and remain stable without the need for an erosion resistant shoal in the middle of the inlet. Both of these studies are quite dated and a follow-up with modern techniques is needed to settle the debate.

[3] dinoloket.nl, ID B02D0111, location (198461, 608680) RD.

[4] ID B02G0261, (200450, 606100) RD and ID B02G0805, (200400, 606750) RD

2.4 Recurved Bar of Schiermonnikoog

Due to the closure of the Lauwerszee in 1969, a recurved bar formed to the NW of Schiermonnikoog as described by Oost (1995, p. 335). The development of this recurved bar can be compared to that of the "Rif"[5], a young supratidal shoal just north of the Engelsmanplaat. The evolution of the recurved bar is therefore described in short below.

Due to the relative increase in strength of waves versus tides, the ebb-tidal delta of the Zoutkamperlaag underwent significant erosion ($26 \cdot 10^6$ m^3 in the period 1970-1987 (Oost, 1995, p. 331)). Oost (1995, p. 335) describes how under wave action the bar grew from a subtidal shoal to a partly supratidal structure (with a maximum height at 1.29 m above NAP based on the 1987 vakloding, see also Figure 5 right panel) from 1979 until 1989. When the bar became supratidal, buildup through wave action decreased, the elongated structure became breached during storms and underwent strong erosion by tides. In 1991 it was again intertidal and in subsequent years fused with the coast of Schiermonnikoog, resulting in a wide beach with a new row of embryonal dunes and a unique "green" beach covered with early stage salt marsh vegetation.

2.5 The Rif

The Rif is a young supratidal shoal with embryonal dunes, a peak elevation of ∼ 2.10 m above NAP and an important breeding ground for terns. Its early growth is analogous to that of the recurved bar discussed in Section 2.4, though the Rif was already present for several decades before the closure of the Lauwerszee. The closure of the estuary however enhanced its growth. It was intertidal in ∼1971, supratidal by 1987 (maximum height of ∼ 1.80 m above NAP) and eroded in the subsequent four years. However, after 1991 it grew in size and height instead of breaching like the recurved bar did. The Rif underwent a merger with an ebb-tidal delta shoal in ∼1995 (see Appendix A Figure 18), with another currently under way. Why the Rif did not erode like the bar at Schiermonnikoog is as of yet unexplained. However, a possible explanation might be the fact that during storm surges, water can flow around the islet due to its small size, in contrast with the recurved bar, which almost completely encloses a 3.3 km^2, 3 m deep lagoon. Winter storm surges are often higher than the maximum elevation of the Rif, thus flooding the islet entirely. However, this washover seems to be concentrated at 199 km latitude as the islet here is roughly 40 cm lower than

[5] "Rif" is a Dutch word for reef, though it is often used to name highly dynamic shoals in and around ebb-tidal deltas. Aside from the "Rif", other examples are the "Noordrif" just north of and partly fused with Rottumerplaat and "Het Rif", a ∼ 4.2 km^2 partly vegetated beach in the southwest corner of Schiermonnikoog.

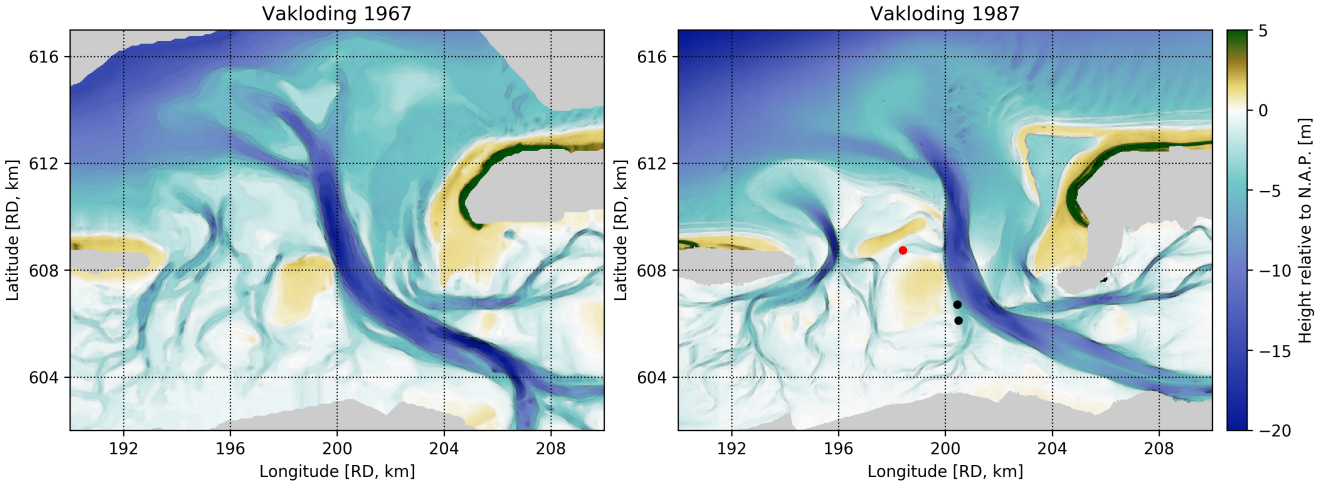

Figure 5: Vaklodingen of 1967, 2 years before the closure of the Lauwerszee, and of 1987, 18 years after the closure. Note the large decrease in volume of the ebb-tidal delta of the Zoutkamperlaag, while that of the Pinkegat remains roughly constant in volume. The drilling performed by Sha (1992)is indicated in the vakloding from 1987 with a red dot. The two other drillings from 1946 discussed here are indicated with black dots.

the highest points on the west and east side (see Figure 4). Furthermore, with high resolution LIDAR altimetry NNW to SSE oriented flow patterns are visible in the area.

The Rif and Engelsmanplaat are seperated by the channel "Oude Smeriggat" (OSG)[6]. It is a remnant of a Pinkegat channel which migrated east through part of the Engelsmanplaat and connected to the Zoutkamperlaag in the 1940's (Oost, 1995, and vaklodingen). It is currently filling up with mud in the summer and sand blown from the Rif and Engelsmanplaat in the winter, though between 1970 and 1987 sedimentation was high with on average $6\,\mathrm{cm\,yr^{-1}}$ (Oost, 1995, p. 264) (see also Appendix A Figure 18). At its shallowest point along the channel axis the Smeriggat's depth was $-2.8\,\mathrm{m}$ relative to NAP in 1967 and $-0.3\,\mathrm{m}$ in 2019.

2.6 Human Interventions

Aside from the closure of the Lauwerszee, several other major human interventions took place. These are natural gas extraction starting in 1986 and sand nourishments at Ameland since the middle of the 1990's.

Natural gas extraction Natural gas extraction from under the eastern side of Ameland and the tidal flats south-east of the Engelsmanplaat has been ongoing since 1986. The areas mostly affected are the dunes and salt marshes of Ameland resulting in relative rise of the groundwater and regression of vegetation in the salt marshes, among other effects (Commissie Monitoring Bodemdaling Ameland, 2017). In several dune valleys over 30 cm of land subsidence was observed. However, the tidal flats have seen no significant change as the sedimentation has kept up with subsidence. This is most likely due to an increase in the tidal prism, enlarging the magnitude of the flow velocities thus raising the sedimentation rate (Wang and Oost, 2011). The dune valleys and salt marshes of Ameland flood less frequently than the tidal flats. They therefore experience less import of sediment, making them unable to keep up with the land subsidence. Overall, the effects of gas extraction on the study area can be safely ignored.

Nourishments Since 1990 sand nourishments have been ongoing throughout the Netherlands to prevent the coastline from retreating beyond a baseline set that year. In the region surrounding the Frisian Inlet nourishments have only been performed at Ameland. An overview of the sand suppletions is shown in Figure 6. Throughout the years the type of nourishments performed has changed. In the early 90's nourishments consisted of transporting sand directly to the dune and beach and using bulldozers to distribute it evenly. Nowadays suppletions are mainly done by dropping sand onto the foreshore and allowing natural processes to distribute it along the beach. This leads to a smaller disruption of the ecosystem, but leaves less control over where the sand ends up. An important unanswered question is whether the sand from nourishments at the barrier islands of the Wadden Sea ends up in the inlets and

[6]The "oude" or old Smeriggat channel OSG; the "new" channel NSG runs roughly north-south to the west of the Engelsmanplaat. The NSG and OSG naming convention started when the buoys of the (old) Smeriggat channel were moved to the NSG around 2008 due to the waterway becoming to shallow. Only the NSG currently bears the official "Smeriggat" name and it is the designated alternative shipping lane.

the backbarrier basins.

2.7 Cyclic Behaviour of the Pinkegat and Engelsmanplaat

2.7.1 Engelsmanplaat

De Haan et al. (1983) describe a 90-100 year cycle in which the Engelsmanplaat changes shape. This is based on historical data on the name of the channel NW of the Engelsmanplaat (now known as the Smeriggat) and hydrographical surveys since 1810. Since at least the 17th century this channel was given a new name in roughly the aforementioned cycle period. Using the assumption that a new name was used every time a new channel appeared, they deduced this ∼95 year period. The hydrographic maps corroborate this period length (see De Haan et al. (1983) p. 54). Oost (1995) derive a varying period length of 50-100 years based on hydrographic maps alone. This cycle can be summarized as follows based on the descriptions of De Haan et al. (1983) and Oost (1995). In brackets are the years between vaklodingen in which the described changes are visible.

1. (1927-1949) While the Engelsmanplaat is firmly supratidal, a shoal ("rif") from the Pinkegat ebb-tidal delta shifts SE.
2. (1949-1967) This shoal squeezes a channel towards the Engelsmanplaat, which also subsequently shifts southwards.
3. (1967-1987) Through wave action the rif becomes supratidal, which blocks the sand supply of the Engelsmanplaat.
4. (1967-1987) The Engelsmanplaat is eroded by wave action from supratidal to intertidal and decreases in surface area.
5. (1987-2002) Further southward migration of the rif causes the channel to quickly fill up.
6. (-) The shoal merges with the Engelsmanplaat, increasing its size.
7. (-) The sand supply from the North Sea is again uninterrupted, allowing the Engelsmanplaat to grow supratidal and develop embryonal dunes.

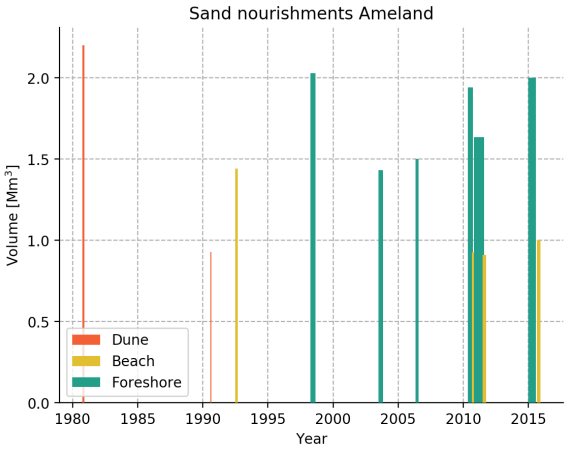

Figure 6: Sand nourishments at Ameland between "raaien"[7] 8 and 22.8 km, corresponding to latitudes 175.7 and 190.5 km. Any sand from nourishments located more to the west is most likely not moved all the way to the Pinkegat by the mean eastward currents. The width of the bar indicates the duration of the nourishment. Data source: Rijkswaterstaat/Deltares Open Earth Portal.

Note that the years 2003 till 2019 are not listed in this summary: since 2002 the Rif has not merged with the Engelsmanplaat. This goes against the prediction of Oost (1995), who expected in 1995 that the Rif will merge with the Engelsmanplaat "in the near future". Is the time needed for step 6 more than 17 years? Will the current cycle be longer than the upper limit of 100 years given by both De Haan et al. (1983) and Oost (1995)?

2.7.2 Pinkegat

Just like the Engelsmanplaat the Pinkegat undergoes a cyclic evolution, though at a different time scale. It is described in detail by Oost and De Haas (1992) and Oost (1995), and consists of three steps:

1. A single large inlet which shifts downdrift to the east. The eastern head of Ameland grows in the channel bend and is eroded in the south by channels in the tidal basin.
2. Several small "embryonal" inlets are formed by cutting through the supra- to subtidal head of Ameland. The eastern channel becomes smaller due to a decrease in discharge.
3. Channel abandonment and merging occurs due to downdrift shift, which is more quickly for the smaller channels. The westernmost inlet increases in cross-sectional area as it shifts eastwards and becomes the main inlet from step 1. The head of Ameland grows starts to grow again.

Overall migration velocity The relative importance of wave and tidal energy dictate the rate of change and the shape of the ebb-tidal delta (Huijs and Lambeek, 1993). At the Pinkegat these two are roughly equal. However, there are large localized differences. For example, sediment transported by waves will settle on the updrift side of an inlet, which will narrow the inlet. This results in larger currents, thus erosion by the tidal current will expand the inlet on the downdrift side. Here, the wave energy is larger at the shoal updrift of the inlet, while in the channel itself the tidal energy dominates (Huijs and Lambeek, 1993). The downdrift migration of

channels at the Pinkegat is influenced by more factors than described in the example above. First of all, as the dominant wind direction is west and the Pinkegat lies east of Ameland, aeolian transport forms an additional sedimentation component. Furthermore, the Coriolis force, which is directed to the right on the northern hemisphere, counteracts the centrifugal force during flood and strengthens it during the ebb (Oost, 1995). This causes additional erosion just downstream of the outer bend in the ebb phase and sedimentation just downstream of the outer bend in the flood phase. As the drainage basin of the Pinkegat is located updrift with respect to the inlet, the ebb and flood flows need to be deflected almost 180 degrees. Therefore, erosion of the outer bends is rather large (Oost, 1995).

Faster migration of smaller channels Smaller channels migrate faster than larger channels due to several factors: 1) the sand supply, which pushes against the channels as a kind of "sand pressure", is mainly from the updrift direction where also the smaller channels are located (Oost, 1995); 2) the smaller channels have a smaller tidal prism, thus the relative strength of waves and sand pressure is larger (Oost, 1995); 3) deeper channels often cut into more solid, semi-consolidated sediments which resist erosion more than the top layers (Huijs and Lambeek, 1993); 4) deeper channels need to erode more sediment on the downdrift side, slowing migration (Huijs and Lambeek, 1993).

Stability and instability of a single inlet A single inlet is generally more stable than multiple inlets due to the larger discharge. However, after merging into a single channel, the inlet slowly migrates eastward which increases the travel time of the ebb and flood currents around the bend. This means that the gradient of the tidal phase difference is decreasing. Van Veen (1936) states that the tidal current will prefer a path with the strongest gradient in phase difference, thus travelling roughly parallel to the propagation direction of the tidal bulge. For the Pinkegat this is NW-SE (Oost, 1995). Therefore, when the single inlet has migrated far enough to the east, the shoal in the inner bend, which is also an extension of the head of Ameland, will be breached.

Evolution since 1994 Currently the Pinkegat is in phase 3 with various merging channels (see Figure 2). In 1987 the system was in phase 1 with a single, large inlet and a single ebb shield visible in Figure 2. The figure also shows two small flood channels west of the main ebb channel. These developed in subsequent years into larger ebb-dominated channels (Appendix A Figure 18). Oost (1995) claim a period of 20 to at most 54 years for the Pinkegat cycle based on data since 1832. They do not make a forecast for the evolution of the system from 1994-1995 onwards, but it seems that their prediction would be that the cycle would continue repeating. Interestingly the throat of the main channel at latitude 608.8 km has not moved further east since 1994 (even moved ∼100 m west) as evidenced by the vaklodingen. Though the channel cross-sectional surface area has decreased significantly, it has not been abandoned. The new main channel of the Pinkegat inlet has been in roughly the same position and remarkably almost exactly the same orientation (NE-SW) since 2000. Will the system merge into a single inlet once again? When this happens, will the duration of this single cycle be within the range given by Oost (1995)?

3 Data

In contrast with other studies which focus purely on the morphodynamics of their respective areas of interest, here we will also place a large focus on the data and processing used. "Big Data" is becoming increasingly important in many scientific fields, including the coastal sciences. A distinction between classical and novel sources of data can be made. Classical data sources often have lower spatial and temporal resolution than the novel techniques, though pitfalls and applications are better known. Examples of classical data types are the vaklodingen, JarKus (yearly bathymetric measurements along the entire Dutch coast) and in-situ sampling (e.g. the SIBES project[8]). The novel data types mainly concern remote sensing, which in essence means that no in-situ measurements are taken. Instead, sensor platforms measure large areas in a single sweep. Examples are satellite imagery of various types (optical, radar, LIDAR) and airplane based imagery (mainly optical and LIDAR). These have the advantage of often having a significantly higher spatial and temporal resolution. For example, the vaklodingen have a revisit period of 6 years, while Sentinel-2 imagery has a (theoretical) revisit period of 5 days.

As with the research objectives, the data sources used and potential extra sources which were not employed here will both be listed. We aim to provide a complete list of sources which could be employed in coastal research because merely trying to find additional datasets and possible applications can take a substantial amount of time and effort.

3.1 Used data

The satellite imagery used for this work was accessed using Google Earth Engine (GEE) (Gorelick et al., 2017), which is free for education, research and non-profit use. It contains a large a diverse catalogue of geospatial products which is easily accessible with

[8] https://www.nioz.nl/en/research/projects/4126-0

Table 1: Parameters of the various optical satellite platforms from which data was used in this work. For clarification on the "effective revisit frequency in ROI" (region of interest) see the main text. Note: before march 2017 when only Sentinel-2A was in orbit, the revisit period of Sentinel-2 was 12 days. Landsat-8 also has a panchromatic band covering the entire optical spectrum with a spatial resolution of 15 m, but it is only available in the TOA data. The revisit period given is valid for the equator. At larger latitudes, images overlap more frequently and the revisit period is smaller.

Satellite/Instrument	Start date	End date	RGB/NIR spatial resolution	Available bands of interest	Revisit period	Effective revisit frequency in ROI
Sentinel-2/MSI	3-6-2015	-	10 m	RGB/NIR	6 (12) days	12 (6) per year
Landsat-8/OLI	1-4-2013	-	30 m	RGB/NIR	16 days	1 per year
Landsat-7/ETM+	1-1-1999		30 m	RGB/NIR	16 days	0.5 per year
Landsat-5/TM	1-1-1999	1-5-2012	30 m	RGB/NIR	16 days	0.5 per year
Terra/ASTER	4-3-2000	-	15 m	GB/NIR	16 days	0.5 per year

the Python API. A large advantage is that the data comes (partly) pre-processed, which is especially useful for the SAR (synthetic aperture radar) data. Cutouts to a specified region of interest are automatically made before the data is downloaded, which drastically reduces the size of the files. This is in contrast with the ESA Copernicus portal[9], which requires users to download and pre-process the raw data themselves.

3.1.1 Optical Satellite Imagery

For the optical imagery four main satellite platforms were used: Sentinel-2/MSI[10], Landsat-8/OLI[11], Landsat-7/ETM+[12], Landsat-5/ETM[13] and Terra/ASTER[14]. An overview of the main parameters of these four platforms is shown in Table 1. One of the most important parameters is the revisit period, which is generally given at the equator. At higher latitudes, images overlap and the revisit period is larger. This is mainly influenced by the swath width, which is the size of the acquired images on the ground perpendicular to the flight direction. The Landsat satellites all have a swath width of 185 km for their main imaging instrument, while Sentinel-2 has a much larger swath width of 290 km. This results in a much larger image overlap. The largest limiting factor in image acquisition is the cloud cover in the region of interest. In the summer this is roughly 44% of the time, while in winter this goes up to about 72%[15]. To properly map the morphology, images must be taken near low tide when the shoals in the inlet are visible, or during slack water in the high tide phase. Both are narrow windows of only roughly 1.5 hours wide, thus only in about 3 out of the ∼13 hours in a tidal cycle the conditions are right for taking an image. This in combination with the high cloud cover decreases the number of high quality images significantly. Note that the best imaging timeframe is the high tide slack water, as the tidal peak is broader at the top than the tidal through is broad at the base. This indicates lower current velocities and thus lower turbidity around high tide than around low tide. Right at the high tide peak, the visibility increases dramatically from less than 0.5 m to ∼6 m. At the low tide minimum the visibility stays roughly at 0.5 m. Therefore, at high tide slack water we can image many of the subtidal features which would not be distinguishable at low tide. This is also shown in Figure 7: there are many more subtidal features visible in Figure 7(b) than in Figure 7(a), though both are taken roughly 40 min before high and low water, respectively.

For Landsat-8, Landsat-7 and Landsat-5 the number of available images per year is 1, 0.5 and 0.5 respectively due to the low revisit period and in the case of Landsat-7, also due to issues with the sensor. The Terra/ASTER imagery was also very sparse at roughly 0.5 useful images per year. These images where strangely much more often affected by clouds than those from the other earth observation platforms. For Sentinel-2 with two satellites in the constellation (thus with a revisit period of 6 days), roughly 12 useful images are available per year. Between june 2015 and march 2017 only a single satellite was available in the constellation, reducing the number of useful images to ∼4 per year.

The spatial resolution of the imagery is quite important as it dictates the positional accuracy and minimal scale of features in the images. As we are interested in large-scale morphological change, a ground resolution of 30 m or less will be sufficient. The smallest channels in the Pinkegat inlet throat are ∼60 m wide and can therefore in theory be imaged at this resolution. However, a higher resolution is generally preferred. The high resolution of Sentinel-2 imagery together with the high revisit frequency makes it the best among all the optical satellite data available on Google Earth Engine.

[9] https://scihub.copernicus.eu/dhus/#/home
[10] Sentinel-2 on Earth Engine data catalogue
[11] Landsat-8 on Earth Engine data catalogue
[12] Landsat-7 on Earth Engine data catalogue
[13] Landsat-5 on Earth Engine data catalogue
[14] ASTER on Earth Engine data catalogue
[15] Source

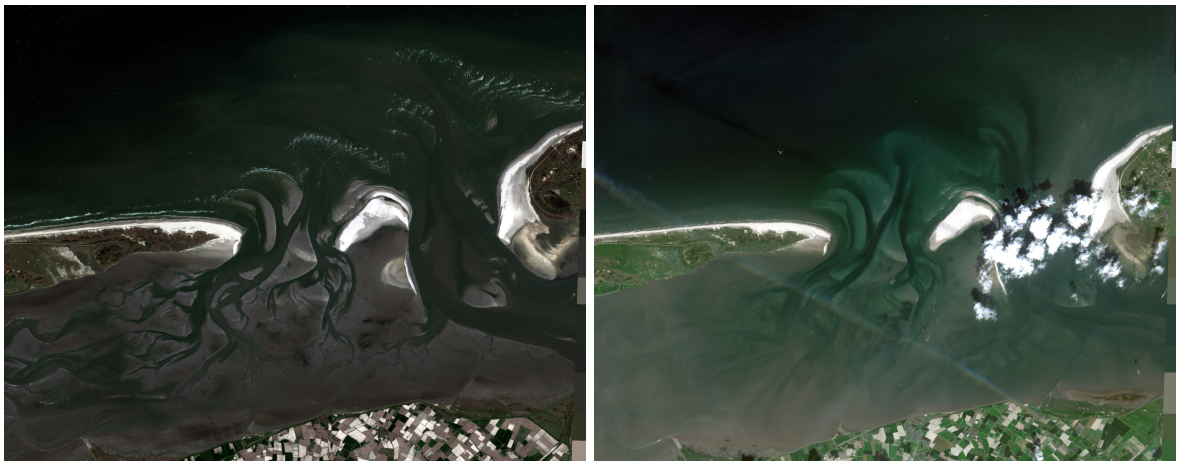

(a) 16-4-2019 low tide

(b) 22-6-2019 high tide

Figure 7: Two Sentinel-2 images taken just over 2 months apart, but one 32 min before low tide (Fig. 7(a)) and one 45 min before high tide (Fig. 7(b)) slack water (tide measured at the ferry terminal of Schiermonnikoog). Many more subtidal features are visible in the high tide image due to the water being clearer. Large sediment plumes are visible in Fig. 7(a) at the ebb-tidal deltas.

3.1.2 Radar Satellite Imagery

In addition to optical imagery, radar data from Sentinel-1 was used. This specific type of radar data is called synthetic aperture radar (SAR), which can achieve significantly higher spatial resolution than normal radar imagery. The advantage of using radar data with respect to optical data is that it is unaffected by clouds or the availability of sunlight on the surface. However, individual images have a large amount of speckle noise, which manifests itself as a grainy salt-and-pepper pattern. It is caused by out-of-phase wave interaction with a target (Qiu et al., 2004). Applying certain filters and stacking several images of the same region by taking the mean or median will reduce the impact of the noise, though both have their downsides. The former reduces the effective spatial resolution, while the latter reduces the effective temporal frequency. For Sentinel-1 the spatial resolution is 10 m, which is sufficient for studying coastal features. The revisit period is 6 days at the equator, just like Sentinel-2. Because change in morphology at the scales we are studying has a corresponding timescale of several months[16], stacking images into 60 day long blocks is acceptable. This reduces the amount of speckle noise greatly, though applying filters on top is also needed to acquire sufficient image quality.

Speckle Filtering The most popular filter used for despeckling SAR images is the Lee-sigma filter (Lee, 1983). It functions as follows: 1) calculate the standard deviation (sigma) of the entire scene; 2) replace each central pixel in a moving window with the average of of only those neighbouring pixels that have an intensity value within a fixed sigma range of the central pixel (Lee, 1983). The Lee-sigma filter was reported to be superior in preserving prominent edges, linear features, point targets and texture information. However, because it uses a fixed sigma for the entire image, it blurs some of the low-contrast edges and linear features (Qiu et al., 2004). Therefore, for this work we opted for the local adaptive median filter by Qiu et al. (2004). The difference between it and the Lee-sigma filter is that it 1) uses a local sigma instead of an image wide sigma; 2) the pixel range is determined by the local mean plus/minus the sigma value instead of the central pixel value plus/minus the sigma value; 3) the central pixel is only replaced if it is identified as speckle noise. Qiu et al. (2004) found that the local adaptive median filter preserves structure and detail better than the Lee-sigma and several other filters. An example of a filtered and median-stacked Sentinel-1 image is shown in Figure 8.

Other Data Characteristics Sentinel-1 has four operational modes, namely 1) strip map (SM); 2) Interferometric Wide Swath (IW); 3) Extra Wide Swath (EW); 4) Wave (WV). IW is the main mode over land and has a 5 by 25 m spatial resolution, which is sufficient for our goals. It also has the highest coverage of the region of interest and therefore the mode used in this report. Optical satellite imagery is often made in multiple wavelength bands simultaneously. For SAR, there is only a single wavelength band or frequency used. In the case of Sentinel-1, this is the C-band at 5.405 GHz (corresponding wavelength of 5.5 cm) (Attema et al., 2007). The penetration depth of radio waves in water is generally rather low. For sea water at room

[16] Excluding storm events with a timescale of a few hours.

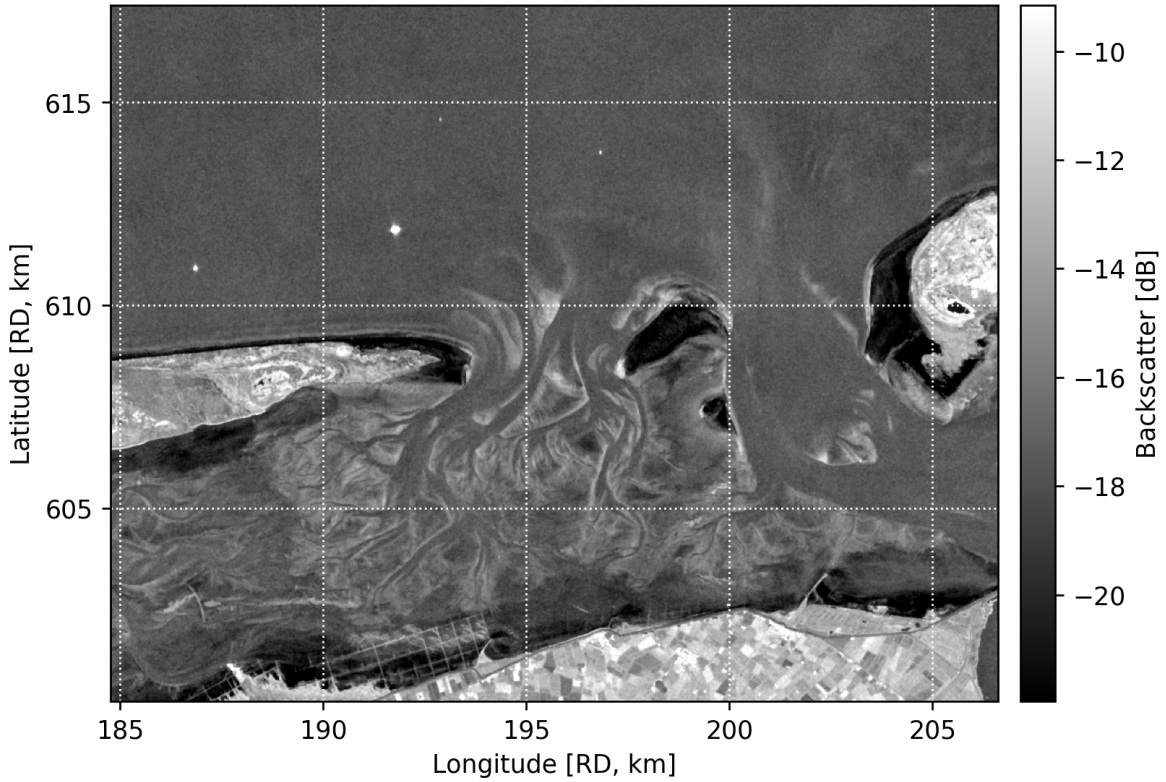

Figure 8: A 60 days median stacked VV polarization image with a 5 by 5 pixel local adaptive median filter applied. The central date is 18-5-2018.

temperature in the C-band this is roughly 4.2 mm (Swift, 1980, Fig. 6). This increases at lower frequencies, but does not go beyond ∼1 cm for saline water. Imaging the bathymetry with SAR at any frequency is therefore completely out of the question.

The polarization of the backscattered light can be used to extract more information. The data in IW mode available through Google Earth Engine contains only the vertical send - vertical receive (VV) and vertical send - horizontal receive (VH) polarizations. The HH and HV polarizations are only used near the poles. A comparison between the two polarizations can yield information on ground cover type as different objects covert vertical to horizontal polarization at different rates. However, the muds and sands in the Wadden Sea barely convert vertical to horizontally polarized light. The VH signal in the inter- and barren supratidal regions in and around the Frisian Inlet is therefore at or below the noise level. Thus only the VV polarization is used for this work.

Signal Strength Regimes The SAR signal S is measured in decibels (dB) having three main signal regimes in the C band:

A) $S > -10\,\mathrm{dB}$: signal double bounce back towards the sensor. Examples: buildings, ships and drilling rigs.

B) $-20 < S < -10\,\mathrm{dB}$: diffuse backscatter in all directions. Examples: plowed fields, tidal flats covered in lugworm excrements.

C) $S < -20\,\mathrm{dB}$: specular reflection of the signal away from the sensor. Examples: undisturbed water surfaces, smooth mudflats.

The main factors influencing the signal strength (here also referred to as "backscatter", though not all the signal is necessarily scattered) are in decreasing order of importance 1) overall surface shape; 2) surface roughness (linked to grain size); 3) surface moisture content. The high signal strength in regime A is caused by a double bounce off of surfaces which are roughly perpendicular to each other, acting akin to a radar retro-reflector on a buoy. These objects can be seen in Figure 8 as four dots off the coast, with the two western dots drilling rigs and the two eastern dots navigational beacons and/or measurement stations. Regime B backscatter is caused by a high surface roughness, scattering the emitted radar pulse everywhere, including in the direction of the spacecraft sensor. In Figure 8 the regime B signal is mainly present in vegetated areas (e.g. dunes and salt marshes), plowed fields and regions in the tidal flats and outer delta's with ripple patterns. The latter mainly produces strong backscatter if the ripples have scales in the order of the radar wavelength. In coastal zones regime C is the most interesting signal range. Water should cause specular reflections and thus signal in regime C. However, Figure 8 shows

that the sea has a moderate signal. This is caused by on average a rough sea surface due to waves. The "Westerplas", a freshwater pond on Schiermonnikoog, is sheltered from the wind and shows very low backscatter, as expected. Some regions of land where one would expect medium backscatter actually belong to regime C, like the barren beaches of Ameland, the Rif and Schiermonnikoog. These generally have backscatter values 2 dB lower than the ponds on the islands. The tidal flats near the islands and the mainland also show low backscatter. The latter is most likely caused by the presence of large mudflats in these regions, which often have a layer of water on top during low tide. Both the water and the small grain size, resulting in a smooth surface, causes the specular reflection visible as a dark spot in Figure 8. The former example of the beaches is puzzling though and as of yet unexplained.[17] The water surface in the region of interest thus shares its backscatter brightness range with many other types of surfaces in the tidal flats. This makes differentiating between the shoals and water, and thus extracting the channels, challenging.

3.1.3 Vaklodingen

The vaklodingen are depth soundings taken throughout the coastal waters of the Netherlands at a frequency of roughly once every 6 years. This dataset is unique in the world as nowhere else the sea floor has been so thoroughly mapped. However, the data does have its own issues. Before 1985 all the data was stored in analog form in the shape of paper maps. These were digitalized in the '90s and all have lower spatial resolution than the digital data from after 1985. An overview of the data till 2001 is presented by de Kruif (2001).

Before 1985 the spatial resolution of the interpolated grid was roughly 250 m squared and after 1985 it is 20 m squared (de Kruif, 2001) (e.g. Figure 5 left versus right panel). The error in the measured depth is heavily dependent on weather, wavefield characteristics and the local underwater topology. It is usually in the order of 10 cm (Wiegmann, 2002). The exact interpolation method used is difficult to uncover. Interpolation errors are often present, for instance in the vakloding of 2019 (Figure 2 in the Pinkegat (RD 195, 608.5 km) and the Westgat (RD 200, 612 km). The vertical accuracy is unknown but most likely in the order of 10 cm. In recent years LIDAR measurements of the shoals have made the depth soundings there more accurate than in the channels. Aside from many of the uncertainties mentioned above, the vaklodingen have one other drawback. Because the measurements have to be taken in fair weather to reduce the vertical errors, measurement campaigns in median sized regions like the Frisian Inlet do not occur on the same day or even the same month. Single vakloding grids are therefore an amalgamation of measurements taken months apart and thus a single observation date cannot be pinpointed[18]. For example, the vakloding of 2019 (Figure 2) uses LIDAR data from 2018 and it is unknown whether the subtidal bathymetry was taken in the winter or summer of 2019, or maybe even somewhere in 2018. As the local morphology is heavily dependant on the season, uncertainties arise.

3.1.4 JarKus

The JarKus[19] measurements are performed yearly along the entire Dutch coast. These consist of aerial LIDAR surveys for the inter- to supratidal parts of the coast and sonar surveys for the subtidal bathymetry. The sonar measurements are performed along tracks perpendicular to the coast with a coast-parallel separation of ∼250 m. The spatial resolution along the track is 10 m and the tracks generally run up to the −8 m NAP line (Minneboo, 1995). This results in the inlets between the barrier islands not being completely sounded. The JarKus data up to and including 2016 goes up to 2 km east from the head of Ameland into the Pinkegat, thus not completely covering the 3.5 km wide inlet. From 2017 onwards the entire distance up to the Rif is covered. However, measurements points are more scarce than near the coast and especially in the north-east section of the Pinkegat ebb-tidal delta, interpolation errors can occur. Just like with the vaklodingen, the error on the measured depth is in the order of 10 cm (Wiegmann, 2002). For many of the years the exact date of bathymetry acquisition is available. This combined with the fact that the measurements are taken every year and for an extended period (ongoing since 1963) makes the JarKus data quite valuable. Both the vaklodingen and JarKus data are available on the Deltares OpenEarth SubVersion server.

3.2 Other Available Datasets

There are several other datasets which will not be employed for this work. However, they might prove useful in follow-up studies or research in other regions of interest.

[17] There are several other curious areas in Figure 8 with an as of yet unexplained backscatter behaviour. The western point of the Rif and the western side of the 90 cm NAP contour of the Engelsmanplaat both have at least a −10.5 dB backscatter. This places them in the vegetation range, though no significant vegetation is present there. The western side of the tidal basin of the Pinkegat shows on average a higher backscatter than the tidal flats west of the Ameland watershed. This could be caused by sandier sediments in the Pinkegat in comparison to the Borndiep basin near the tidal divide.

[18] Adding an extra layer to the grid indicating the measurement date would alleviate many of the problems, but is unfortunately not available.

[19] "Jaarlijkse Kustmetingen"

NAM LIDAR To monitor the land subsidence as a result of gas extraction, the NAM, which carries out the drilling operations, conducts aerial LIDAR measurements from the watershed of Ameland to that of Schiermonnikoog twice a year starting in 2010. The quality of the data has improved significantly over the years. The first dataset of 2018 generally has a vertical accuracy of 5 cm or better, with only a few locations with a higher error (NAM, 2018). Measurements are done during low spring tide to ensure that the largest possible area of tidal flats can be imaged. This dataset is particularly useful when monitoring the tidal flats, but of less interest for this work. This is due to the fact that we are investigating the behaviour of the channels, not the tidal flats. The channels only appear as large flat regions in the LIDAR datasets and are not directly imaged. Optical satellite imagery provides a way to look lower than the water level at the time of data acquisition, thus enabling imaging of multiple channels in a single inundated region (e.g. the channels just off the coast of the island head of Ameland). The area monitored by the LIDAR measurement campaign is the backbarrier basin of the Friese Zeegat (Pinkegat and Zoutkamperlaag) up to the throat of the inlet. The behaviour of the inlet itself and the ebb-tidal delta is therefore difficult and/or impossible to trace.

Aerial Imagery The entire Netherlands is imaged yearly using aerial photography with a spatial resolution of 4 to 10 cm in the winter and early spring and with a resolution of 25 cm in late spring and the summer. The high resolution dataset consists of RGB images but is not open to the public. The low resolution dataset consists of RGB and NIR images and is open data, but unfortunately only available for the 5 most recent years on a WMS server (not available in GeoTIFF format). This makes a "big data" approach with automated downloading and processing near impossible. Furthermore, the 5 most recent years of data would not add much value as in this period Sentinel-2 already provided high quality and regular data. Finally, the exact imaging time and date is not available for the aerial imagery, while this is crucial to construct a morphological timeline and to take summer/winter patterns into account.

SAR Interferometry The data from the SAR platform Sentinel-1 and processing thereof have been described in Section 3.1.2. However, one important aspect of the data which was not covered is the phase information in the imagery. In addition to measuring the backscatter, the SAR sensor on board the Sentinel-1 satellites also measures the phase of the incoming light wave. By comparing the phase of each pixel in a region in two successive passes, one can build up an interferogram. This shows the shift in phase between the two imaging dates. Knowing the wavelength Sentinel-1 operates at, one can determine the vertical displacement of the Earth's surface between the two dates. An example of a large scale approach is Zinno et al. (2018), who made a displacement velocity map for Italy. The same techniques could be used to monitor the sedimentation and erosion of the inter- and supratidal shoals in the entire Wadden Sea with a vertical accuracy of ∼5 mm. This would be tremendously useful for the NAM, as this presents a much higher vertical accuracy and temporal frequency than the LIDAR measurements. However, processing the data is arduous and has to be completely done by the user as Google Earth Engine does not currently provide the phase data.

Other Optical and SAR Data Sources There are many other satellite remote sensing platforms which have produced data possibly useful for this research in the past. However, the data of most of them is not available through the Google Earth Engine. The data portals of the individual providers are often not compatible with big data type of processing (e.g. having to manually download every image) and tough to work with (e.g. the ESA SNAP toolbox). Regarding SAR, the RADARSAT-1, Envisat/ASAR, ERS-1 and ERS-2 missions all supposedly have data publicly available. Incorporating these datasets in an analysis would enable one to study morphological evolution at high temporal frequencies from 1991 until present. For optical imagery one could use data from Planet, which provides 3 to 5 m resolution RGB-NIR near daily imagery. Planet has the downside that it is a closed data source (students and researchers can only download a minimal amount of imagery each month), but the higher temporal frequency enables a critical selection of images. This could drastically improve satellite derived bathymetry estimates and improve the timescale at which changes in the Wadden Sea are observed. Planet also has a Python API, enabling downloading data at a large scale.

4 Methods

This section is split into three, covering processing of optical data (Section 4.1), radar (SAR) data (Section 4.2) and other processing techniques which are promising for future research (Section 4.3). The former two are also presented separately in subsequent sections.

4.1 Optical Satellite Imagery & Bathymetry

There are three products we want to extract from the optical data. 1) RGB images for a complete picture of the changes in the region of interest; 2) transects of the green band through the Pinkegat inlet; 3) a map of the centerlines of the channels

in the inlet and backbarrier basin throughout the years. Images for these products are selected using the following steps:

1. Region and cloud cover ($< 20\%$) filtering using the built in GEE functions FILTERBOUNDS() and FILTERMETADATA() respectively.
2. As GEE does not provide a native ROI coverage check, a custom made one is performed in the cloud. It compares the total area of the ROI to that of all the pixels with a value larger or equal to 1. If the area covered by the image is larger than 70%, the image passes the test. This works for all five satellite platforms.
3. A cloud cover test is performed again, but this time with the quality assurane (QA) bands of Sentinel-2 and the Landsat satellites. Terra/ASTER does not provide a QA band and this step is therefore skipped for this satellite platform. The same cloud cover threshold as before is used. Because the GEE FILTERMETADATA() cloud cover filter does not eliminate all images with a high cloud cover this manual check filters out a large portion of images.
4. Finally, all images are audited by eye to filter out images where 1) the cloud cover is higher than predicted by the image metadata and QA bands; 2) where a small amount of clouds covers the inlet itself and 3) where the suspended sediment concentrations in the channels at the Pinkegat inlet are too high to image underwater morphology.

The resulting selection for the green band transects consists of 44 images between the dates 13-5-2000 and 31-8-2019: 11 from Terra/ASTER, 5 from Landsat-5, 7 from Landsat-7, 4 from Landsat-8 and 17 from Sentinel-2.

RGB Images For the RGB images the main processing consists of atmosphere corrections which is effectively colour balancing, and scaling the data values to pixel values. The atmospheric corrections usually consist of complex models of the atmosphere at the time of image acquisition, which specific parameters for these models extracted from the different image bands. These corrections therefore convert an image of detected light at the Top-Of-the-Atmosphere (TOA) to an image measuring the solar light Surface Reflectance (SR). The corrections have already been applied to the Landsat data, so SR data for these satellite platforms is available. However, the dataset of Sentinel-2 SR on GEE barely contains any images, thus we have to rely on the TOA imagery. For Terra/ASTER there is no SR catalogue available. Applying the atmospheric correction with these intricate goes beyond the scope of this work. Instead, we can make use of a key characteristic of our region of interest: deep water. The surface reflectance of very deep water should be zero excluding foam and specular reflections, as the water attenuates all the incoming light. Any light in pixels over deep water are therefore caused by the aforementioned or the scattering of light in the atmosphere. By clipping each RGB band between the 0.5 and 99.8% percentile of the respective bands, the scattering of the atmosphere is practically removed. As an additional enhancement, the image values, when scaled to the interval $[0, 1)$, are processed by a power law transfer function $f(x) = x^{0.6}$. This ensures that dark pixels appear less dark, thus resulting in more underwater features being visible while preserving adequate image contrast. Clouds and breaking waves in some cases cause problems in determining the upper limit with the 99.8% percentile. Therefore, the image is masked using the cloud masks given by GEE and by applying a maximum on the pixel entropy, determined in a 3 pixel radius, of 3.5. The former masks large parts of clouds and their shadows, while the latter masks thinner regions of clouds which are not detected by GEE and masks the foam of the breaking waves. A comparison between the different processing step is shown in Figure 9.

In the case of Terra/ASTER, there is no blue band available, so a NIR-RG image is made instead.

Green Band Transects For the transect timestack of the optical satellite images, we only use the green band data as this penetrates deepest through the water column. The green band image is first re-scaled using the tanh function to the range of $(-1, 1)$:

$$G_{scaled} = \tanh\left(\frac{G_{raw} - \overline{G_{raw}}}{\sigma_G}\right) \tag{1}$$

where $\overline{G_{raw}}$ is the mean and σ_G is the standard deviation of all the pixels of the raw green band image. This scaling is different from the transfer function applied to the RGB image as this enhances dark pixels even more, increasing contrast in deep underwater regions. For the RGB images the visual appeal of the image warrants the use of the power law transfer function. The image is subsequently smoothed using a 2D gaussian with a standard deviation of 0.5 pixels. This removes a large part of the noise in the image, which smooths out the transect, while mostly retaining the effective image resolution. The transect values are extracted from the raster image using a nearest neighbour search along the transect path.

There are four transect paths used for determining the channel migration behaviour in the Pinkegat inlet and the migration of the Rif. For the first, three transects are used, one covering the inlet throat (transect "A"), one arcing slightly north of the throat ("B") and one arcing stronly north ("C"). The last transect, "D", runs perpendicular to the NW

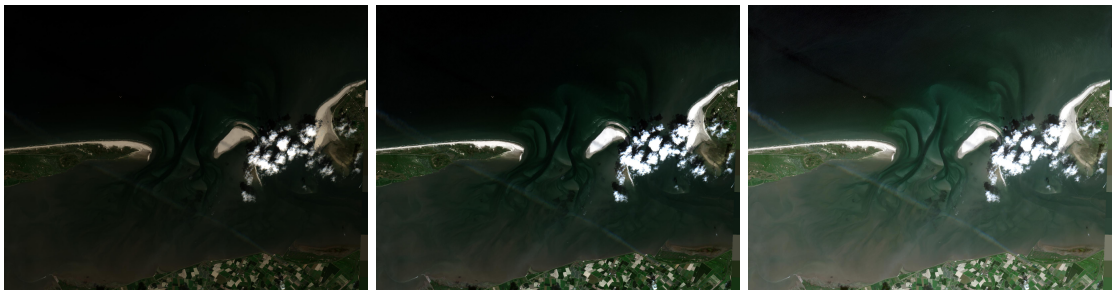

(a) Only percentile min/max (b) Added cloud masking (c) Added transfer function

Figure 9: Comparison of the various preprocessing steps taken for the RGB images. The image itself was acquired by Sentinel-2 on 22-6-2019 50 minutes before high tide at the ferry terminal of Schiermonnikoog (not visible in image, source: waterinfo.rws.nl). The third panel shows the morphology of the submerged shoals in the Pinkegat inlet most clearly. It also shows that in the inlet the tide is in the slack water phase, containing a very low amount of suspended sediment. Further into the backbarrier basin, the suspended sediment concentration is visibly higher, indicating that the slack water phase has not yet arrived there.

coastline of the Rif. The exact transect paths are presented in the figures in the results section.

Centerline Detection The transects described above only provide a 1D view of the channel migration. Channel rotations and abandonment are more difficult to distinguish in the transects, so a 2D map of the channel axes or centerlines is also made. This is also done for the SAR data, but it uses a more complicated processing pipeline which is described in the following subsection. The steps for the green band centerline detection are given below:

1. All the green band images are upsampled to the Sentinel-2 10 m resolution using the Python package Pillow's IMAGE.RESIZE() function using a nearest neighbour resampling filter. This is done as the final centerlines will be provided as a binary raster image and stacking these is easier when the spatial resolution is equal.
2. The green band image is smoothed with a gaussian kernel with a radius of 2 pixels to prevent many small undesired centerlines from appearing later in the process. The location of the centerline of the main channels is largely unaffected by this processing step.
3. The image is scaled using Equation 1.
4. All pixels with values below -0.35 are classified as water and everything else classified as land; this produces a binary image.
5. Small regions classified as water and small islands are removed to improve the centerline map results. This is done because if for example a patch of high turbidity water in a channel is classified as land, the channel centerlines will run around both sides of this island. This creates a large deviation from the actual channel axis.
6. Morphological thinning is applied to the binary image using SKIMAGE.MORPHOLOGY.THIN() to produce a centerline map. The centerlines are single pixel thick lines in a raster image of the same shape as the original green band image.
7. The centerlines are pruned using a custom algorithm to remove all lines shorter than 35 pixels (at the Sentinel-2 spatial resolution) and those that run straight vertically or horizontally with a cross-track/alongtrack ratio greater than 0.8. This pruning algorithm is run twice to remove small trees of undesired centerline branches. The same algorithm is used for the SAR centerline detection pipeline described later on.

Note that due to irregular shapes being present in the binary classification image mainly seaward of the inlet throat, an enormous amount of centerlines might be produced. Pruning is therefore required to make a practical centerline map.

Vaklodingen & JarKus Just like for the green band transects, the bathymetry based on the vaklodingen and JarKus data is scaled using Equation 1 to simplify plotting both in a single image. These transects are plotted together with the green band transects to provide an overview of the morphological changes in the Pinkegat in the period 2000 to 2019. The transects are plotted in a timestack manner, with each transect having a different vertical displacement in the plot to represent the days between the data acquisition dates.

4.2 Radar (SAR) Processing

VV Transects After median stacking and speckle filtering, as described in section 3, the data is first scaled using Equation 1. It is subsequently smoothed

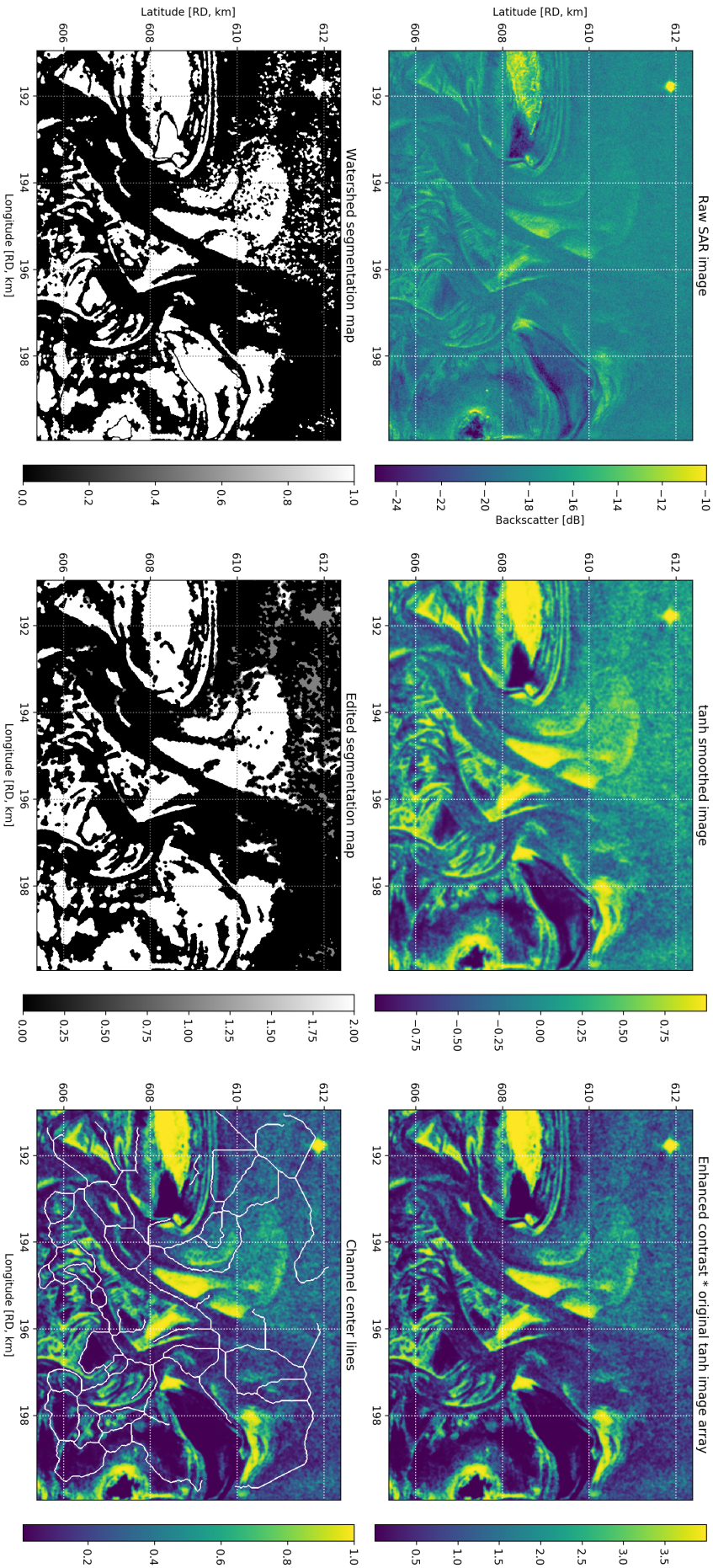

Figure 10: A visualization of the various processing steps for the centerline detection in a Sentinel-1 SAR image.

with a gaussian kernel with a radius of 2 pixels. This is crucial when obtaining SAR transects as the speckles will otherwise cause extremely large bumps in the transect itself, while a smooth profile is needed to detect the channels (whether automated or by eye). As with the green band and bathymetry transects, the SAR transects are stacked vertically to better disentangle the different dates.

Centerline Detection Detecting the channel axes in SAR imagery is much more challenging than in optical images, as the channels are not characterised by very low pixel values. Instead, as described in section 3 and illustrated in Figure 8, intertidal areas can have both low and high pixel values while the channels and sea have mid-range pixel values due to wave induced sea surface roughness. The processing steps required for a proper centerline map were devised through trial and error, and are briefly outlined below. These steps are visualized in Figure 10.

1. The raw data, which is the 60 day median stacked VV polarization image (Figure 10 top left panel), is rescaled using Equation 1 and subsequently smoothed using a gaussian kernel with a standard deviation of 2 pixels (Figure 10 top center panel). These are the same steps as steps 2 and 3 of the green band centerline detection process.
2. A high contrast version of the image is made using a custom filtering algorithm comparable to SKIMAGE.FILTERS.RANK.ENHANCE_CONTRAST. This is multiplied with the tanh scaled image to provide a middle ground between enhancing contrast and resolution (Figure 10 top right panel).
3. A primitive segmentation map based on thresholding is made to provide a starting point for a watershed algorithm. This algorithm is run two times to generate a segmentation map for both very dark and very bright regions in the image. Small dark regions at sea are removed by applying a morphological opening operator (SKIMAGE.MORPHOLOGY.OPENING) to the dark region segmentation map. The two segmentation maps are subsequently combined by addition. In this way the bright and dark regions are combined to form the "land" segment. The medium brightness region is the "water" segment. See Figure 10 lower left panel for the result of this step.
4. The current segmentation map is of acceptable quality in the basin, but at the ebb-tidal delta and at sea the large amount of wave scatter causes many small islands to appear. To combat this, a large amount of processing steps are performed. First of all, the pixels with wave influence are detected using a wave mask. For the wave mask, the entropy of the entire image is determined in 3 by 3 pixel windows and smoothed with a gaussian filter with a size (standard deviation) of 1.5 pixels. Edges in the image are detected using a sobel edge detector and dilated with a circular kernel with a radius of 5 pixels. The image entropy is then corrected for edges by subtracting the dilated edge map. We also want to preserve regions where there are a large number of breakers due to subtidal shoals, as these provide information on the underwater morphology. Therefore, the tanh scaled image from step 1 is smoothed using a gaussian filter with a size of 5 pixels and subtracted from the entropy map. All pixels with a (corrected) entropy map value larger than 2 are classified as wave dominated.
5. The wave mask in its current state classifies many crucial regions in the basin as being wave impacted. To combat this, a morphological dilation with a kernel with a radius of 2 pixels is applied, and small islands and holes in the mask are removed. With this adjusted wave mask the segmentation map is changed to indicate water (value 0), waves (value 1) and land (value 2). This segmentation map is shown in Figure 10 lower center panel.
6. As a final processing step before determining the channel centerlines, small holes in the land and small islands in the water regions are removed. The segmentation map is compressed to a binary land-water classification image by merging the wave and water regions.
7. The centerlines are determined using SKIMAGE.MORPHOLOGY.THIN. The resulting centerline map is pruned using the algorithm described previously for the green band centerline detection. For visualization purposes in Figure 10 lower right panel the centerline is dilated with a circular kernel with a radius of 1 pixel. The enhanced contrast image from the top right panel is normalised and used as a background.

Migration Velocity The migration velocity of channels on a transect can be determined by matching successive centerlines, thus creating a position-time (x, t) diagram. The migration velocity between pairs of known centerline positions is then easily obtained by calculating the numerical derivative $\left(\frac{\mathrm{d}x}{\mathrm{d}t}, t\right)$.

4.3 Other available techniques

The data used in this work can be employed to extract much more information than described here. This is beyond the scope of this work, but helpful to list for follow-up research. One major technique that could be applied to the optical and infrared data is satellite derived bathymetry. Using theoretical extinction laws for water or empirically derived relations, one could derive a bathymetry map using the

RGB and NIR bands of a satellite image. This has already been proven in regions with clear water, for example at coral reefs and in the Caribbean. However, developing these algorithms for regions with generally high suspended sediment concentrations like the Wadden Sea is much more difficult.

The suspended sediments themselves could also be mapped using satellite imagery, producing a kind of turbidity index akin to the normalized difference vegetation index (NDVI). Calibrating this index with measurements from a field campaign timed to satellite image acquisition dates and times could enable instant precise mapping of suspended sediments in large regions.

One could use waterlines from the normalized difference water index (NDWI) in combination with the known tidal water height at tidal gauges in the Wadden Sea to determine intertidal bathymetry contours. The NDWI is a commonly used index for differentiating between land and water, though we noted that it also consistently detects intertidal areas as a third class. As stated before (Table 1), Sentinel-2 produces roughly 12 images per which are suitable for mapping subtidal morphology. However, for mapping the intertidal bathymetry contours one does not require low turbidity, thus bumping up the number of available images to at least 16 per year. This allows one to derive the complete intertidal bathymetry due to the high sampling resolution on the complete tidal range in a single year. For the Frisian Inlet this is not necessary due to the bi-yearly LIDAR measurements by the NAM, but in other regions of the Wadden Sea and beyond this could be a valuable source of tidal flat height data.

Another parameter which could be derived from satellite data is the sediment grain size. As stated previously, the radar backscatter magnitude is partly determined by the grain size of the scattering surface. Van der Wal and Herman (2006) combined this with Landsat-8 spectral information to derive the sediment grain size on a tidal flat in the Westerschelde estuary. The Wadden Sea is a perfect test bed for these technologies because as a part of the SIBES project there have been yearly measurements of the sediment grain size in the entire region. De Vries et al. (2019) derived sediment grain size and benthic fauna biomass from Sentinel-2 spectral data. A map of the sediment grain size could show the redistribution of sediments on tidal flats due to wave action and the effects of storms on ebb-tidal delta shoal migration, among others.

In many of the Sentinel-2 images large swell waves can be clearly distinguished. The change in wavelength and wave direction as the wave traverses the shallow coastal zone is linked to the local water depth. It could therefore be employed to derive subtidal bathymetry between depths of roughly -15 and -5 m.

5 Results & Discussion

5.1 Channel Naming Convention

To properly discuss the channel migration in the Pinkegat inlet, a consistent and clear naming scheme is required. We propose one based on the earliest year of appearance in nautical or bathymetric maps, or satellite imagery. As this yearly data is not (readily) available before the year 2000, the year of appearance of channels and thus the channel name is not exactly known. However, this is not regarded as a major problem because almost all the channels currently present have formed in the period since 2000. In this period the observation cadence is high enough to prevent these naming errors. It can be safely assumed that in the future the regularity of satellite imagery will increase even further and extensive catalogues of old imagery will be available such that no naming errors caused by a lack of data will arise. The naming scheme is given by the following template:

PG-
[yr]<intrayr>/<merged channel yr+intrayr>/...~
<merger yr>/...-
<abandonment yr>

where everything between [square brackets] is a required field and everything between <triangular brackets> depends on the appearance of other channels and merging behaviour. Specifically:

- [yr]: the year that the channel first appeared in the aforementioned sources, e.g. PG-70 for a channel which appeared in 1970. Channels will be named in west to east order.
- <intrayr>: an extra index in the case that two channels appeared in the same year, e.g. PG-70a and PG-70b.
- <merged channel yr+intrayr>: the appearance year of a channel that this channel has merged with. After each subsequent merger the appearance year is appended here preceded by a /.
- <merger yr>: the year that the merging took place. For each subsequent merging event the mergning year is appended, preceded by a /.
- <abandonment yr>: the year that the channel got abandoned.

An example name is PG-70b/75=79-82: a (fictional) channel which was the second to appear in 1970, merged with a channel from 1975 in the year 1979 and got subsequently abandoned in 1982.

The starting point for the naming scheme will be the vakloding from 1987 (see Figure 5). In this year, the Pinkegat was in a single inlet state and thus only a single channel needs to be named: PG-87. When channels merge, parts of the old channels will generally remain in place for a few years down- and

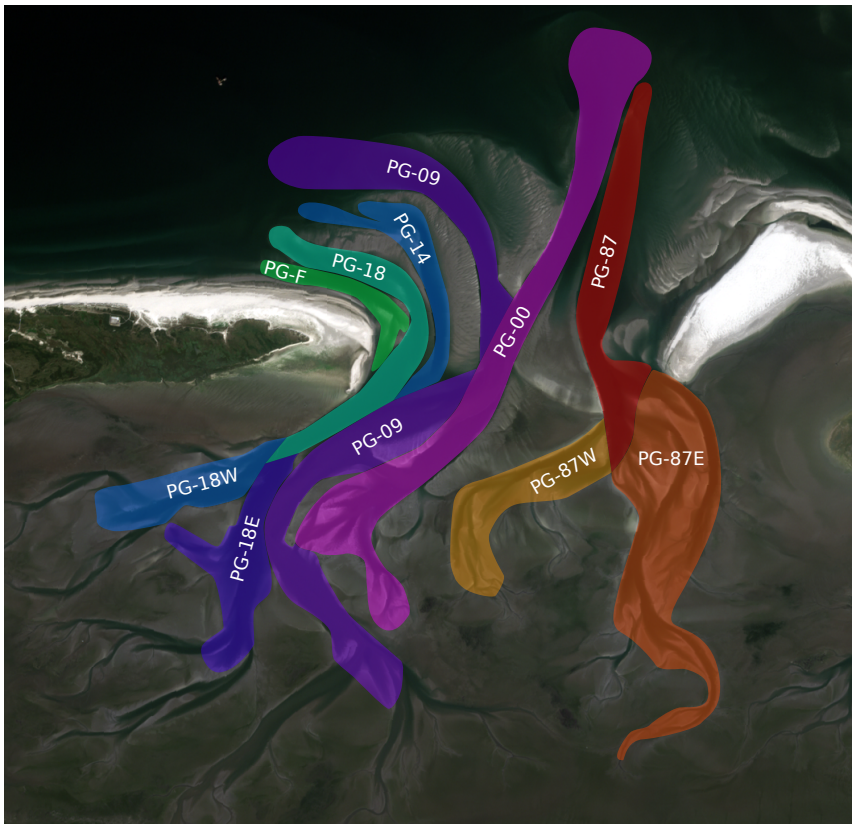

Figure 11: An overview of the names assigned to each channel in the Pinkegat inlet using the naming scheme from Section 5.1 based on a Sentinel-2 satellite image from 26-8-2019. The borders of channels in the western side of the basin touch each other on top of water bodies, because flows merge and then diverge again. These borders were drawn using sediment flows visible in satellite imagery which indicate the separate (non-mixing) water flows. Changes are rapid and therefore difficult to track. For example, the southern basin section of PG-09 used to be a part of PG-00 as recently as 2016 (see also Appendix A Figure 19). PG-F is a flood channel (hence "F") just off the coast of Ameland from which the new channels like PG-18 form. This channel was always present in the period 2000 - 2019, though not always visible in the satellite imagery.

upstream of the merging location. Therefore, the channel name is only valid for a specific location or transect perpendicular to the channels in the inlet. We will most often use the Pinkegat inlet throat, which is defined by the transect between (193, 608.6) and (197.8, 608.6) km in RD coordinates.

Based on the vaklodingen, PG-87 is the easternmost channel in the year 2000 and has not yet undergone any mergers at the inlet throat. In the vakloding of 1991, one channel just off the coast of Ameland is visible: PG-91. In 1994 this channel has migrated eastwards and west of it another channel formed,: PG-94. In 1997 PG-91 seems to be abandoned → PG-91-97. The inlet now consists of PG-87 and PG-94. PG-94 quickly becomes NNE oriented in 2000 and shifts further east, with another channel forming: PG-00. The inlet in the year 2000 therefore consists of three channels from west to east: PG-00, PG-94 and PG-87 (note: unmerged). A map of the named channels for 2019 is shown in Figure 11.

5.2 RGB Image Series

Figure 19 in Appendix A shows a selection of RGB or NIR-RG images of the Frisian Inlet between the years 2000 and 2019. Up to and including 2015 there is roughly a single image shown per year, as more high quality imagery was generally not available. From 2016 onwards more images are generally shown, due to the higher effective imaging cadence of the Sentinel-2 mission. It shows the speed at which some changes occur. For example, between 6-8-2018 and 17-11-2018 a merging event occurs between the two channels west of PG-87 (which is in 2019 still the easternmost channel in the Pinkegat).

This RGB image series serves two main purposes: 1) tracing the evolution of the shape of the supratidal regions in the Frisian Inlet (Rif, Engelsmanplaat and to a smaller extent the eastern head of Ameland) and 2) providing a detailed catalogue for explaining changes which are difficult to follow in the transects alone. The image series shows an overall SE migration of the Rif, with two sets of shoals from the

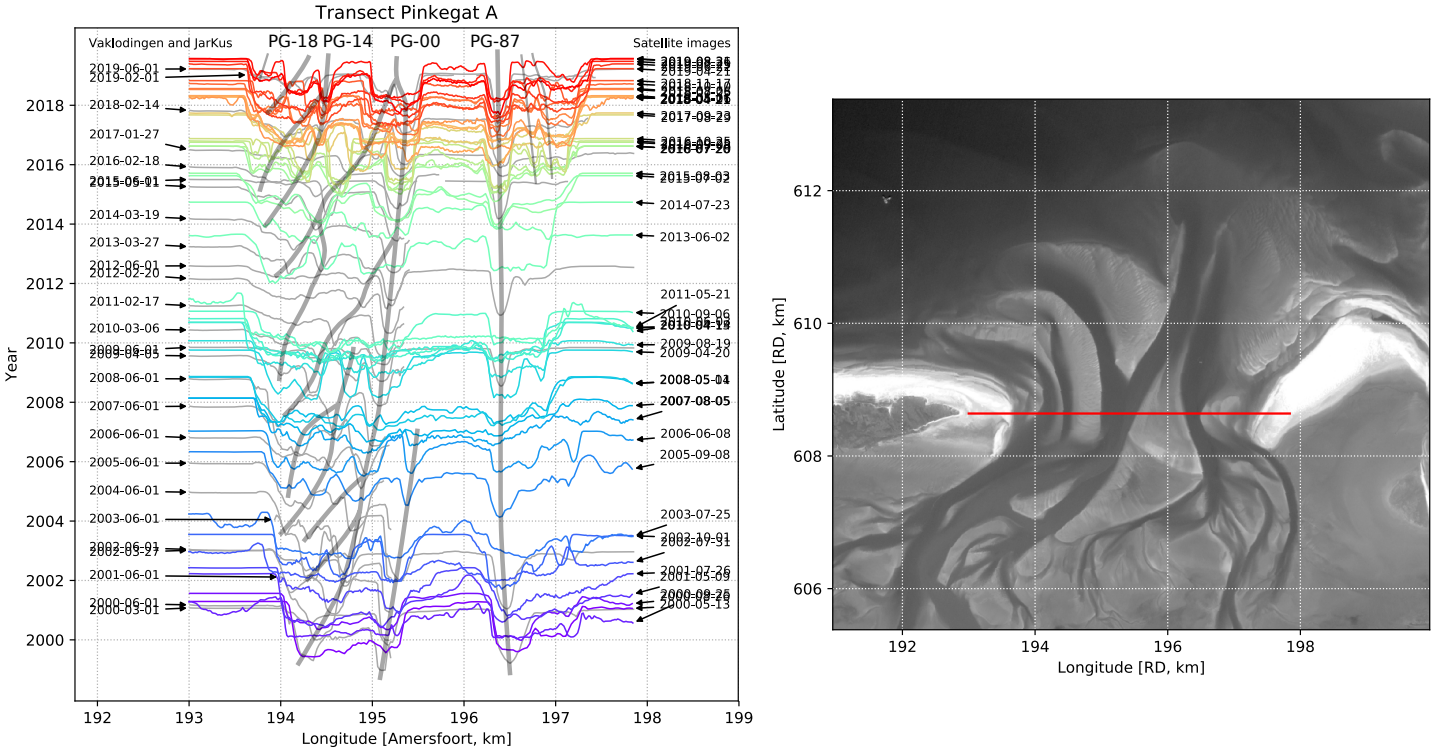

Figure 12: The green band optical transects along path A, the inlet throat from (193, 608.6) to (197.8, 608.6) km. Large ebb channels have been annotated with a broad gray line and smaller ebb channels with a narrow gray line. These smaller ebb channels are quite short (400 m at most) and have a prominent ebb chute. Examples are the channels on the transect indicated in the left panel at longituge 196.8 km.

ebb-tidal delta of the Pinkegat migrating southwards and subsequently shifting eastward in the periods 2000 (or just before) - 2005 and 2013 - 2019. In the periods during the shoal landings the Rif had a very peculiar shape: a straight NW facing shore and a NE facing shore. In the years between the two shoal landings (2005 - 2011) the Rif was very rounded and kidney-shaped. This is the classical shape of a supratidal sandbar in a coastal zone, with a famous example being Noorderhaaks (SW of the island Texel). The ebb-tidal delta shoals facing the Rif became increasingly important, first visible in 2013. The Rif subsequently develops a more angular shape as wave sheltering occurs and sediment from the ebb-tidal delta merges with the islet. The shoal landing is preceded by migration of the PG-87 channel mouth to the SE, caused by wind driven migration of the shoal between PG-00[20] and PG-87. Between 2011 and 2013 this shoal is breached by PG-87, freeing the northern section from the NW directed ebb-flow pressure and allowing it to quickly migrate SE. This is a typical sediment bypass event. The shoal landing visible in the earliest images are a result of the shoal bypass visible in the vaklodingen of 1982 and 1987 (Appendix A Figure 18). This in turn was caused by PG-87 merging with the easternmost channel in the Pinkegat inlet.

In the image series the supratidal (> 90 cm NAP) area of the Engelsmanplaat gradually shrinks from 103 ha to 46 ha and moves to the SE. This does not include the Hiezel itself, the split on the eastern side of the Engelsmanplaat. It has moved southwards by roughly 1 km between 2000 and 2019 and at roughly constant height (140 to 160 cm above NAP respectively based on the vaklodingen). The Engelsmanplaat has remained just above the mean high water level with a height of roughly 100 cm above NAP. However, on its western side it has developed a berm at the mean high water level mark which is visible in Figure 19 as a bright outline.

5.3 Green Band Transects

5.3.1 Inlet Throat Transect

The optical green band transects across the inlet throat (transect A) are shown in Figure 12. The ebb channels which could be distinguished, are annotated with gray lines. The three initial channels, PG-87, PG-94 and PG-00 all start as gray lines at the bottom of the graph. PG-87 is still present at longitude 196.4 km, having only moved at most 50 m westward since 2000. PG-94 can be denoted PG-94-07 as it got abandoned around 2007 when an ebb-tidal shoal between PG-00 and PG-87 moved south (see Fig-

[20] The exact evolution of this channel will be described in the following subsections.

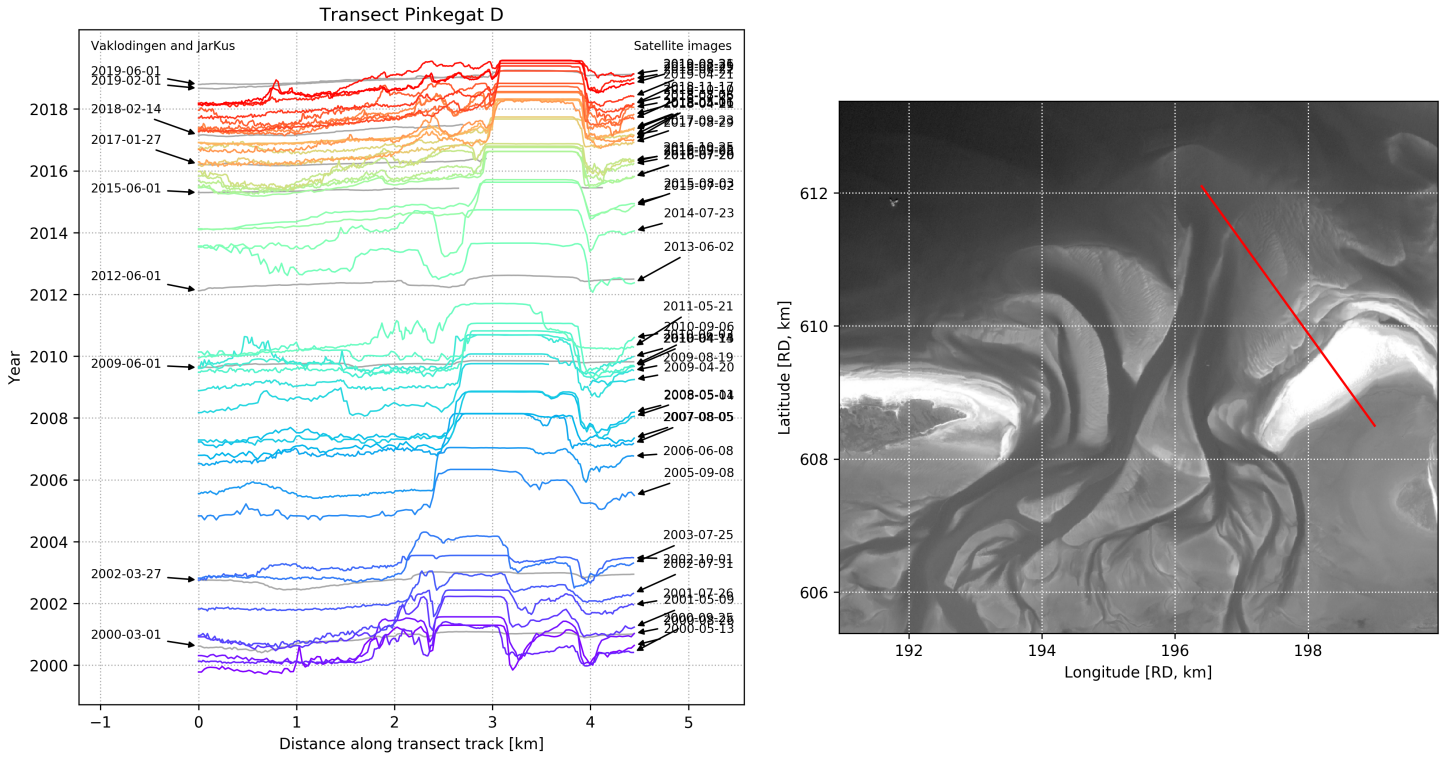

Figure 13: The green band transects along the second path running perpendicular to the NW shoreface of the Rif in 2019. The coordinates of the endpoints are (196.4, 612.1) km and (199.0, 608.5) km.

ure 19). The other channel that got abandoned is PG-04a/05=08-10 between two branches of PG-00. Since 2007, PG-00 is the next door neighbour of PG-87 and has underwent four major merging events: in 2004, 2005, 2013 and 2018. The last channel that PG-00 joined with (PG-09), also underwent such an event in 2014 with PG-13, resulting in PG-09/13=14. The complete name for PG-00 would therefore be PG-00/02/04b/07/09=04/05/13/18, which we will abbreviate to PG-00 (keeping only the index of the first channel that appeared). Note the omission of the merging event of PG-09 with PG-13 in the name. Including this is impossible at is it a second order merging event (akin to a second order branch point in a tree) while all other merging events of PG-00 are first order (the channels it has joined with have not undergone mergers themselves). Aside from PG-87 and PG-00, there are two other channels present. PG-14/15=18 and PG-18. The entire history of channel migration in the Pinkegat inlet between 2000 and 2019 can therefore be described with the following names (excluding second order mergers) sorted by age:

- PG-87
- PG-94-07
- PG-00/02/04b/07/09=04/05/13/18
- PG-04a/05=08-10
- PG-14/15=18
- PG-18

Between 2000 and 2019 new channels were continuously formed and no single channel became dominant in the inlet during this period. (Oost, 1995) concluded that the cyclic development of the Pinkegat has a period of at most 40 to 50 years. A single channel configuration would therefore be expected in roughly 2030. The current situation also looks a lot like the one in 1982, just a few years before the single inlet phase (Appendix A Figure 18). There a large channel from the west with a counterclockwise curvature also approached an older channel in the east with a clockwise curvature, which is analogous to the situation with PG-00 and PG-87 respectively. PG-00 therefore seems the most viable candidate to become the major inlet channel in addition to its size and many past merging events. However, no progress towards the channel inlet configuration has been made since 2000. The inlet still consists of three major channels located at roughly the same position as the three channels in 2000. PG-00 may be abandoned in the near future just like PG-94 was at roughly the same position as PG-00 currently resides. Furthermore, new channels are currently still being formed just off the coast of Ameland. Past channels which formed there when PG-00 was at roughly the same position, like PG-07, needed roughly 7 years to merge with PG-00. Therefore, PG-18 might merge only in 2025, but then new channels could have been formed too. PG-00 will also have shifted further east by then, increasing

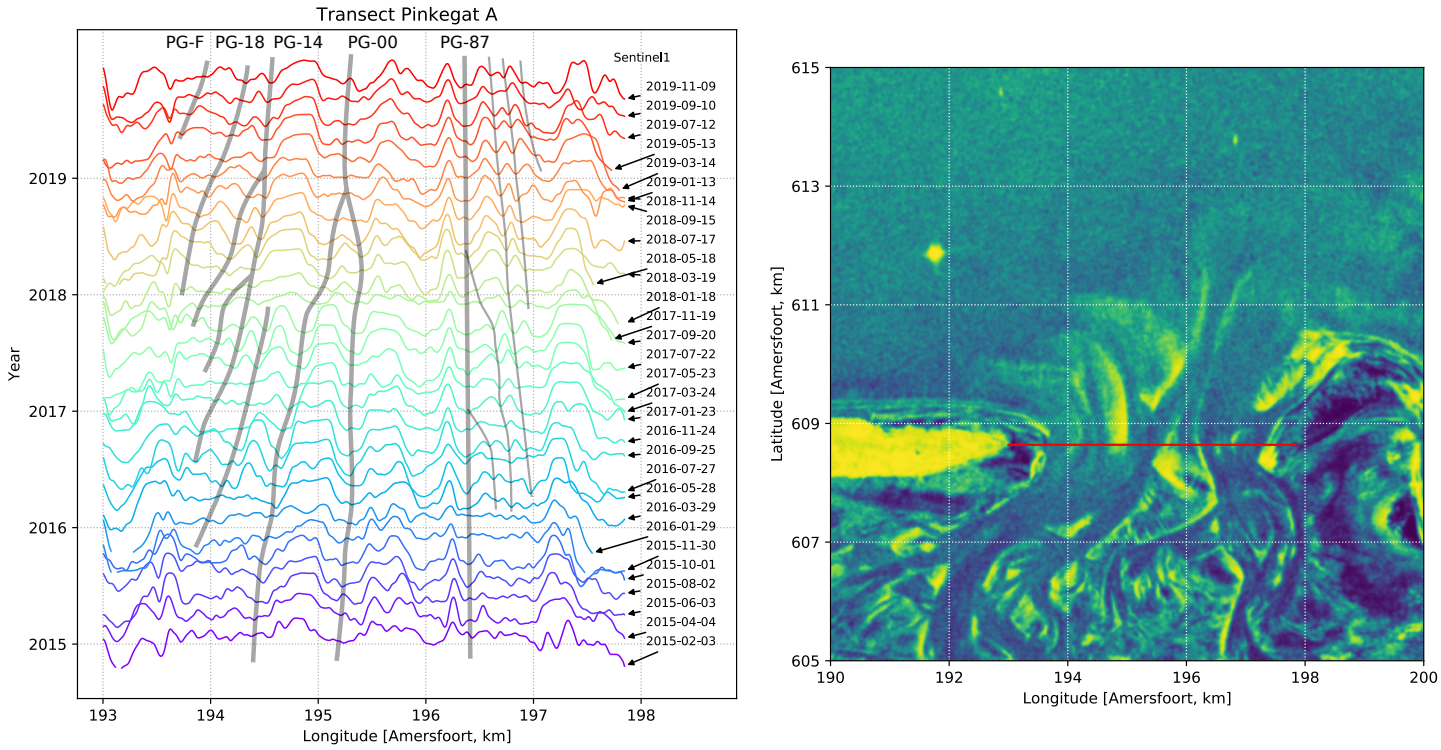

Figure 14: The SAR transect across the inlet throat. Major ebb channels are indicated with thick gray lines, minor ebb channels with thin gray lines. The coordinates of the endpoints are (193.0, 608.6) km and (197.8, 608.6) km. This is the same transect path as used in Figure 12. The image in the right panel is the 60 day median centered around 9-11-2019.

the time until a merging event. Thus, at least one other channel will most likely exist west of PG-00 up until the end of the 2020's. Lastly, PG-00 has been migrating significantly slower in the past 10 years than before. Its average migration velocity between 2010 and 2018 was $\sim$20 m yr^{-1}. At this rate it would take another 37.5 yr to migrate through the shoal separating PG-00 and PG-87, assuming the latter does not move in the mean time and the eastward velocity of PG-00 does not decrease further.

Another point to note is that the eastern head of Ameland has eroded by about 500 m in the period covered by Figure 12. The SE migration of the Rif since 2010 resulted in a widening of the inlet by 500 m. Both phenomena are visible as a shift in the edges of the plateaus at the two ends of the transects in Figure 12. The inlet has therefore widened from 2.9 km to 3.9 m in 20 years. This is indicative of the multiple channel phase, as the erosion of Ameland is thought to be caused by the newly formed channels (Oost, 1995). However, these channels did not form as spill-overs as claimed by (Oost, 1995). Instead, they simply formed from the flood chute just off the coast of Ameland (see Appendix A Figure 19), which is a standard feature of a tidal inlet[21].

[21] Tidal inlets in mixed-energy regimes generally have a central ebb channel and two flood channels flanking the ebb channel, just off the coast of the barrier islands. An example is Fitzgerald et al. (1984, Fig. 7).

Between 2014 and its merger with PG-00 in 2018, PG-09/13=14 was moving at an extremely high pace to the east. At its peak in 2016 its mean migration velocity was roughly 260 m yr^{-1}, compared to 160 m yr^{-1} in the years up to 2015. Only channels such as PG-2 and PG-04b moved at roughly the same rate. These both had a much lower cross-section and tidal prism as well as being more updrift than PG-09/13=14 and should therefore migrate quicker (Section 2.7.2). The cause could be a higher sand pressure due to excess sand from the nourishments in 2011, 2012 and 2015 (Figure 6). However, other causes cannot be excluded as of yet.

5.3.2 Perpendicular To The Rif

The second transect, running perpendicular to the NW shoreface of the Rif in 2019, is visible in Figure 13. It contains less bathymetry transects due to the fact that most of the JarKus measurements do not extend this far from the shoreline of Ameland. However, the main point of interest, the migration of the Rif, is clearly visible in the green band. The quality of such transects is also much less affected by turbidity and tidal water level. Figure 13 shows that the Rif has been retreating to the SE since 2005 with a steady pace of $\sim$48 m yr^{-1}. The SE side of the Rif has not moved further into the direction of the OSG (remained at the 4 km mark along the transect) since

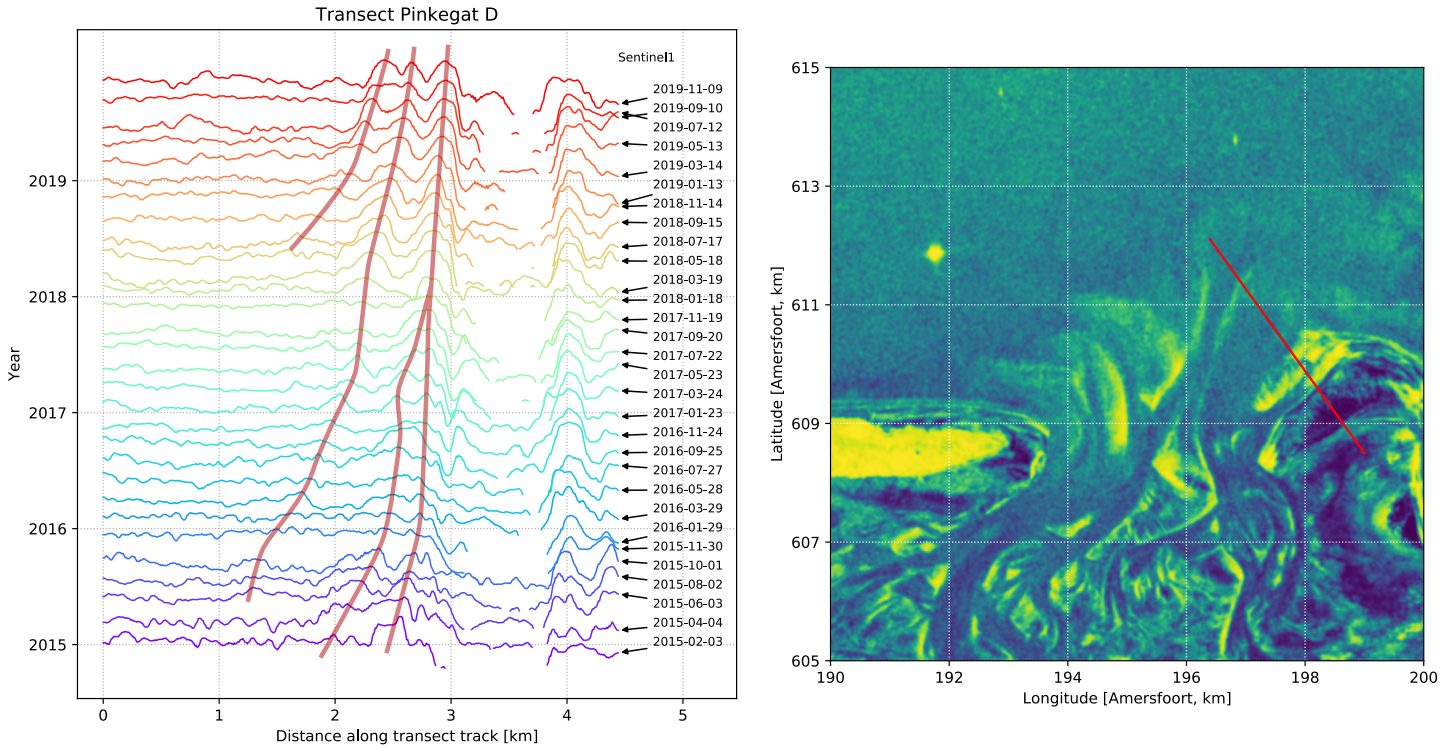

Figure 15: The second SAR transect timestack perpendicular to the Rif's NW shore in 2019. Red lines indicate the sandbars off the coast of the Rif.

2005 and has only steepened. The result is that the Rif has become more narrow over the years, from 1500 to 830 m. This has allowed small ebb channels and tills to form just west of the Rif in the Pinkegat inlet throat. To the NW of the Rif a large set of sandbanks currently resides. When these fuse with the Rif, it might grow further north and become wider again. The same occurred in the period 2000 - 2002 when sandbanks extended roughly 500 m to the NW and their subsequent merger caused the Rif to temporarily grow by 300 m (see the transects from 2003 to 2007).

De Haan et al. (1983) and Oost (1995) both state an upper limit to the period of the cycles of the Engelsmanplaat of 100 years. The current Rif originated in the 1920's (De Haan et al., 1983) as a shoal from the ebb-tidal delta of the Pinkegat. In this period the Engelsmanplaat was not bounded to the north by any shoal other than its own shelf extending roughly 2 km out to the sea. To finish a cycle, the Rif would need to completely merge with the Engelsmanplaat, yet it is far from doing so in its present state. If the northern shore keeps the same migration pace and the southern shore starts to shift south as well (optimal case), then it will take roughly 20 years to bridge the 1 km gap between the two shoals. The cycle would therefore be $\sim 20\%$ longer than expected in the best case. Furthermore, De Haan et al. (1983) and Oost (1995) clearly state that the Rif is expected to merge with the Engelsmanplaat and subsequently form new embryonal dunes. However, the Rif already hosts embryonal dunes with *Elytrigia juncea* (Sand couch) since 2012 and its height is higher than that of the Engelsmanplaat at its peak (210 cm NAP of the Rif now compared to 187 cm NAP of the Engelsmanplaat in 1967. Note that in this period the local sea level has risen by roughly 10 cm (CBS et al., 2018), so the Rif relative peak height is 13 cm higher than the Engelsmanplaat peak height in 1967. The total volume of the Rif above 0 cm NAP is roughly $3.3 \cdot 10^6$ m^3, which is unlikely to all shift south in a single decade. As discussed in Section 2.5, the Rif grew dramatically due to the closure of the Lauwerszee and the subsequent wave-driven landward migration of the ebb-tidal delta of the Zoutkamperlaag. This might be the cause of the larger than expected size of the Rif and thus explain why it has not yet merged with the Engelsmanplaat. As this "sand boost" of the Rif coincided with the phase of the Engelsmanplaat cycle where the Rif should become intertidal, this was not recognized earlier. It could have been simply masked by our expectations of the growth of the shoal.

5.4 SAR Transects

5.4.1 Inlet Throat Transect

The SAR VV polarization 60-day median image transects along the inlet throat are shown in Figure 14 with channels indicated in gray. The higher temporal resolution of this data compared to the optical

data has the advantage that individual channels are much easier to track. When the temporal resolution is lower, the shift of a channel between two subsequent satellite images might be large enough to place this channel at the location of another from the previous frame. This can cause confusion regarding channel identification, which occurs regularly in e.g. Figure 12. The higher temporal resolution of the radar data decreases this channel confusion. However, not every dip in radar brightness is a channel (see Section 3.1.2). Most notable is the section at longitude 196 km at the latitude of the transect path. This part of the shoal between PG-97 and PG-00 consistently has a low backscatter for unknown reasons. A thorough comparison between the transect, SAR image and optical images is therefore required before classifying the channels in the timestack.

For the analysis of Figure 14, let us first focus on the minor ebb channels at longitude ∼196.8 km and the Rif. In the green band transect timestack across the inlet throat, these small ebb channels are visible since 2016. In the SAR transects, these also start in 2016, but two merging events with PG-87 are visible. As these are only minor, secondary ebb channels, they will not be included in the naming scheme. It is however interesting that they only formed recently. This is most likely due to a combination of mainly tidal and mainly wave driven forces: 1) in recent years PG-87 is curved to the NE and will therefore not migrate eastward; 2) the Rif has migrated eastward at the location of the inlet throat due to wave action. These two factors formed a relatively flat section in the inlet which was promptly filled by these secondary ebb channels. Their behaviour, visible as westward migration in Figure 14, was already described by Van Veen (1950). Though in this case instead of disappearing, the minor ebb channels which are the most downstream merge with PG-87. The westward migration velocities of these minor channels are generally $\sim 100\,\mathrm{m\,yr^{-1}}$. They merge with PG-87 within 60 days when their centerlines are separated by less than ∼200 m (and their banks by ∼70 m, though this is more difficult to measure), as evidenced by the mergers at the start of 2017 and 2018.

The eastward migration of the Rif is more difficult to trace than the migration of the channels, as it can have varying backscatter magnitudes. The western head of the Rif generally has a high backscatter though. Assuming this high backscatter spot traces the western head well, we can derive an erosion rate of $\sim 43\,\mathrm{m\,yr^{-1}}$. This is comparable to the SE migration velocity of the Rif since 2005 derived from Figure 13.

The merging event of PG-00 with PG-09/13=14 (abbreviated as PG-09) can be pinpointed more accurately to November 2018. A careful examination of the RGB images confirms this, but their more irregular shape and spacing in the green band timestack makes finding this exact moment in Figure 12 more difficult than in Figure 14. Before merging, PG-09 clearly shows a seasonal change in its migration velocity. In the summer, it is roughly $155\,\mathrm{m\,yr^{-1}}$ (e.g. the summer of 2017) and in the winter it can go up to $760\,\mathrm{m\,yr^{-1}}$ (e.g. the start of 2018). PG-09 has these speed-ups at the start of 2016, 2017 and 2018, and PG-00 has these at the start of 2016 and 2018, though with smaller velocities than PG-09. One should note the behaviour of PG-09 and PG-00 at the start of 2018: they both suddenly migrate faster than in previous winters, especially PG-00. This delayed the channel merging by about 6 months. PG-87 does not shown any speed-ups and has a mean velocity of 9 m per year westward. This confirms the theory from Oost (1995) that channels located more towards the island head of Ameland migrate quicker.

The higher temporal frequency of the SAR data with respect to the optical data reveals more small channels just off the coast of Ameland, but recognizing them is much more difficult. The PG-18 channel from the optical transects is also visible in Figure 14, as well as the most western channel in 2019. In 2019, the PG-16/17a/17b=18/19 channel in the SAR transects (abbreviated as SAR PG-16) corresponds to the PG-14/15=18 channel in the optical transects. The origin of this channel is therefore disputed between these two datasets. One may consider the possibility that the SAR channel PG-15-17 actually merged with SAR PG-16. However, the individual 60 day median images show that PG-15-17 got pushed north, transformed into a flood channel and got abandoned in the end of 2018. PG-15-17 could have formed in 2014 already, only becoming visible in late 2015 in the radar imagery. This can be explained by the fact that the westernmost channels have very small ebb-tidal deltas, so large waves can penetrate these channels more easily. These waves cause a higher backscatter in the channels themselves, reducing the contrast between the channels and the shoals. The same could have occurred with SAR PG-16, making it appear a year later than PG-15 in Figure 12. SAR therefore improves mapping of all the channels due to the higher temporal frequency, but the small, westernmost channels sometimes slip under the radar due to the higher wave-induced backscatter.

5.4.2 Perpendicular To The Rif

Just as with the optical data, a transect timestack is made perpendicular to the NW shore of the Rif (Figure 15). We can observe the changes in the sandbars and the change in shoreline position of the Rif. There are currently three sandbars located NW of the Rif which are also visible in the RGB images (Appendix A Figure 19). They also light up extremely well in the SAR image in the right panel of Figure 15. These sandbars migrate faster

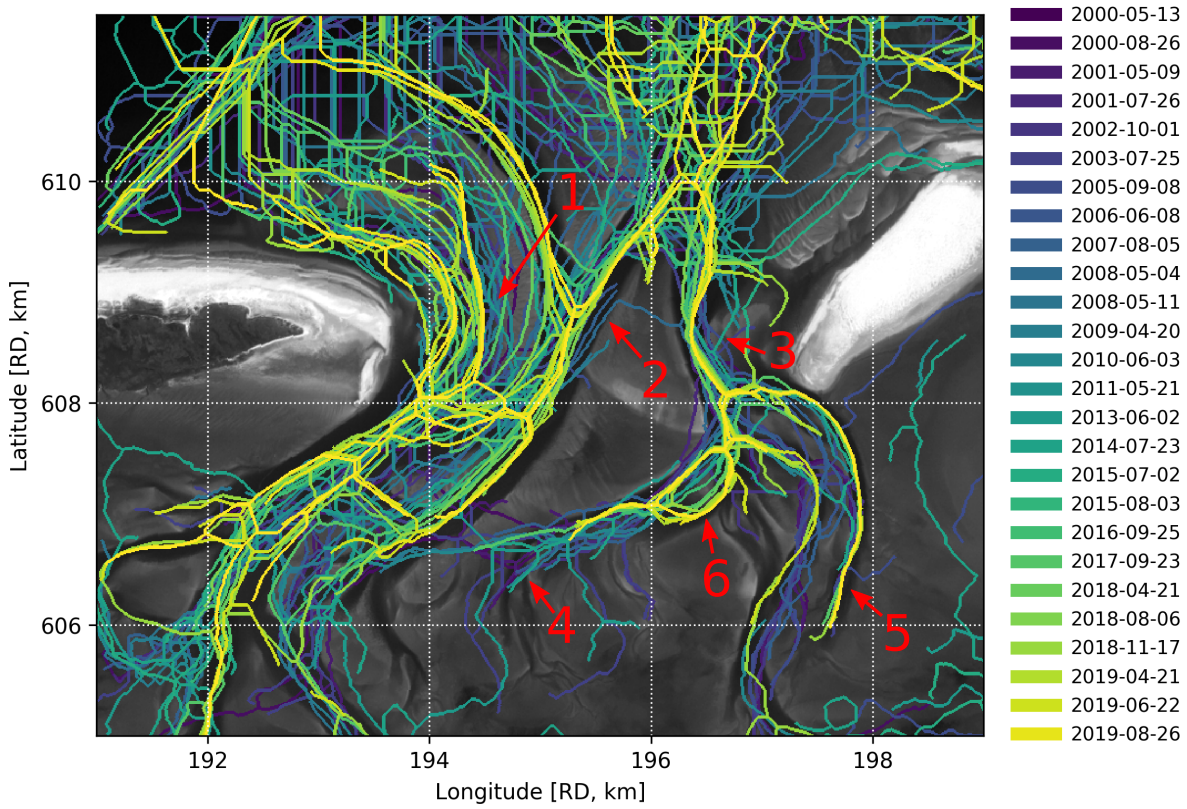

Figure 16: A map of channel centerlines detected in optical imagery between 2000 and 2019. The background image is the green band of the Sentinel-2 image from 26-8-2019. Regions of interest are indicated with numbers.

when they are further away from the shoreline and nearly always migrate towards the shore. The only exception is the central sandbar at the start of 2017 when it moved slightly seaward. For subtidal and intertidal sandbars at gently sloping coasts it is known that they generally migrate shoreward in the summer and seaward in the winter (Gallagher et al., 1998; Masselink et al., 2006; Ruessink et al., 2009). The latter occurs primarily during high waveheight events such as storms. It is however not known if sandbars such as those at the Rif have the same behaviour. The shoals of the ebb-tidal deltas of the Pinkegat and Zoutkamperlaag shelter these sandbars against high waves, possibly reducing the impact of storms on their migration.

Characterizing the erosion of the Rif is much more difficult here than with the green band images, as the backscatter around the shoreline varies and does not show a plateau like in Figure 13. Nonetheless, by looking at the VV polarization images themselves, we can derive a reasonable shoreline definition, namely halfway between the peak of the closest sandbar and the low values of the main body of the Rif. Using this definition, we estimate an erosion rate of $\sim$34 m yr^{-1}, which is 29% lower than the estimate using the green band transects. Note that shoreline positions are easier to track in the optical data than the radar data. Therefore, the former is preferred when tracking supratidal shoals.

5.5 Centerline Maps

5.5.1 Green Band Centerline Map

The green band centerline map in Figure 16 has a large amount of overlap between each successive centerline. This mainly occurs in the western section of the inlet throat (region 1 in Figure 16, between 193.5 and 196.0 km longitude) and in the same channels up to 3 km into the basin. At the edge of the ebb-tidal delta many straight vertical centerlines can be seen, which are incorrect detections. A large portion of these were filtered out with the pruning algorithm described previously, though evidently not all could be removed. At the Engelsmanplaat a network of centerlines from a single date can be seen. These are likely due to a high amount of algae covering the tidal flat and resulting in a false channel detection. False centerlines are therefore a reoccurring problem in these maps and caution in the analysis should be taken.

At the inlet throat (region 1) PG-09 can be seen moving at a rapid pace east around 2016 and merging in 2018 with PG-00. To the west two channels, PG-14/15=18 and PG-18, can be seen quickly forming and migrating eastward. Below the centerlines of

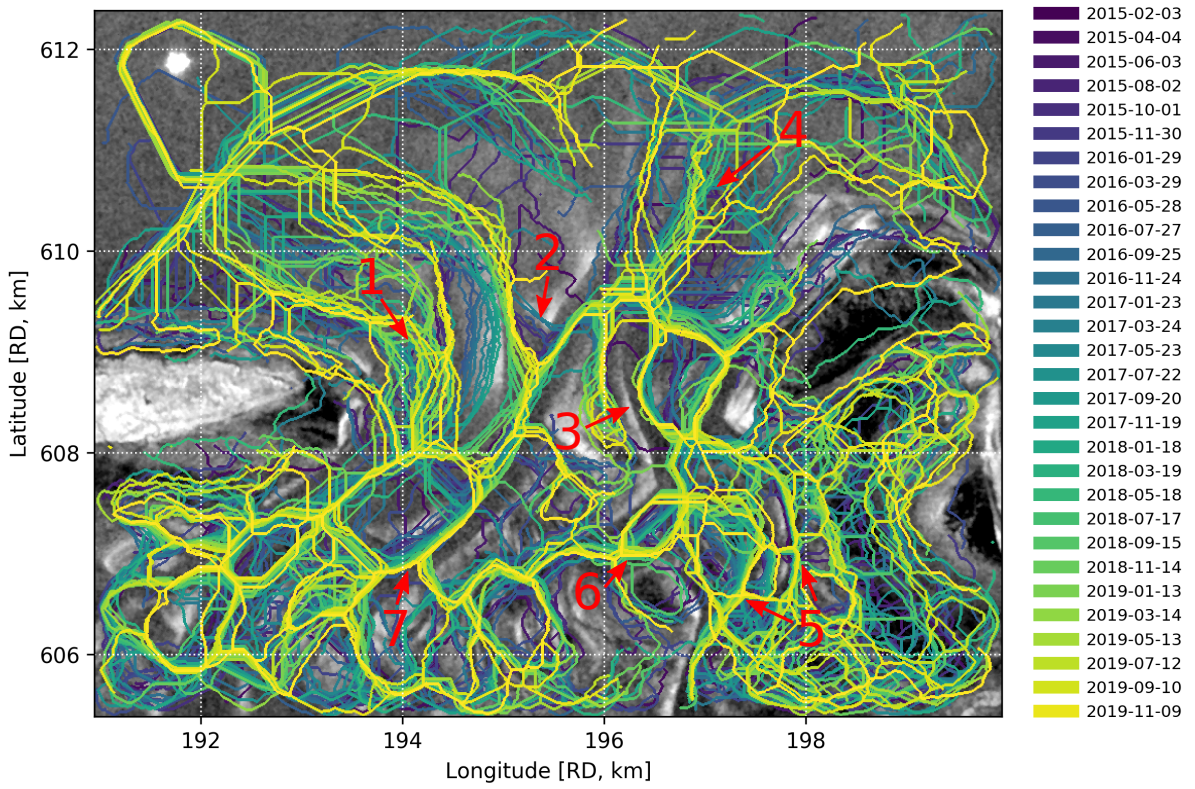

Figure 17: A map of channel centerlines detected in Sentinel-1 SAR imagery between 2015 and 2019 with a cadence of 60 days. The background image is the VV polarization 60 day median image centered on 9-11-2019. Note that this image has a slightly larger extent than the optical channel centerline map in Figure 16. Regions of interest are indicated with numbers.

these two recent channels, centerlines of older channels which merged with PG-00 and PG-00 itself can be seen. These are best visualized in the transect in Figure 12. Below the recent centerlines of PG-00 at roughly 195 - 195.5 km longitude (region 2) the centerlines of PG-94-07 can be seen. A single centerline at (196.0, 609.0) km indicated by the arrow of region 2 alludes to the demise of this channel: it rotated clockwise due to a shoal pushing in from the north around 2006 until running nearly east-west. It subsequently got abandoned and the shoal migrated further south until merging with the already present intertidal (∼65 cm NAP high) shoal in 2013. PG-00 is currently at almost the same location as PG-94-07 when it silted up. As posed in Section 5.3.1, it might therefore undergo the same fate as PG-94-07. This is especially the case as it recently merged with PG-09 and can shift its drainage to this more westerly channel in the ebb-tidal delta. The configuration of the channels is highly similar to that in 2003. The channel abandonment back then was inevitable from 2008 onwards. Therefore, in five years we can draw conclusions on whether PG-00 will undergo the same fate.

At exactly the inlet throat[22] (region 3) PG-87 is nearly stationary for the last 10 years. Centerlines from 2000 - 2010 sometimes lie more towards the east. This can be attributed to high tide and high turbidity, making the flooded inlet appear larger and blocking the view of the underwater morphology, respectively. Such cases limit the accuracy of a centerline map. Just north of the throat two series of clockwise migrations of PG-87 can be seen. The first series ended in 2015, resulting in a shoal bypass forming the supratidal sandbank currently present just north of the Rif[23]. We could therefore be seeing a new steady state: channels migrating east and getting abandoned like PG-94-07 and PG-87 "wagging its tail" with shoal bypass events.

In the currently examined timeframe since 2000 PG-87 has gradually lost part of its backbarrier basin to the more western channels. This is visible in Figure 16 as the western basin channels of PG-87 ("PG-87W") at region 4 became shorter and lost their connection with the basin channel of PG-00. This resulted in a generally more NW directed momentum of the water during the ebb phase, allowing it to shift from N-S oriented to SE in the basin. The Smeriggat (region 5, the easter basin channels PG-87E) developed a complex system of ebb and flood channels, in contrast with the year 2000 when

[22] Defined as transect A in Figure 12, running due east from the easternmost dunes of Ameland.

[23] Unofficially the "Buitenrif".

there was only one major ebb and one major flood channel present. The easternmost ebb channel of the Smeriggat migrated towards the NE between 2000 and 2013 and has since remained stationary. A new, more western located ebb channel formed since ∼2012. Note that the southern part of the eastern Smeriggat ebb channel PG-87E has not migrated towards the Engelsmanplaat since the start of our satellite image sequence. The continued erosion of the Engelsmanplaat on its western side expected by Oost (1995) has therefore not taken place. The eastern channel of PG-87E will most likely be overtaken by the western channel of PG-87E.

PG-87W (region 6) shows a textbook meandering pattern. Starting nearly straight in 2013, it has developed a single full oscillation in 2019 (195.2 to 196.7 km longitude). The eastern bend of PG-87W is being cut off in the inner bend since 2018. The same meandering action can be seen in the most western basin channel of PG-14/15=18 and PG-18. Since ∼2007 it has slowly (∼30 m yr^{-1}) been migrating NW. There is no significant erosion at the southern side of the Ameland island head.

5.5.2 SAR Centerline Map

The SAR centerline map, which spans a smaller timeframe and contains a higher imaging cadence of 60 days compared to the green band data, is shown in Figure 17. There are far less incorrect centerlines at the ebb-tidal delta than in the green band centerline map. The extensive wave filtering and pruning described in Section 4.2 has paid off. As the SAR imagery has a constant imaging cadence, the centerlines for migrating channels show a smooth spatial colour gradient. On the other hand, the incorrectly detected centerlines on the tidal flats in the south and east do not show this smooth gradient. This enables one to recognize them easily by eye. There are several regions with notable changes which are discussed separately below in a clockwise order.

The channels just east of Ameland (region 1 in Figure 17) are difficult to detect as they are extremely dynamic, sometimes undergoing mergers every 6 months. The image cadence is once every 2 months, thus sometimes only 3 images between mergers. Some images have lower contrast between the shoals and the water, resulting in less images where these small channels are detected. The result is a forest of centerlines which does not show steady trends. Just to the east (region 2), the channel PG-09 shows a steady eastward migration trend with a merger in the autumn of 2018. The pre-merger migration velocity was on average 200 m yr^{-1} encompassing 9 centerlines, equivalent to 18 months. This is in accordance to the velocities derived from the transects in Section 5.4. PG-87 migrated ∼30 m westward at the inlet throat (region 3) in the measurement period of nearly 5 years. This movement might be caused by slight variances in the creation of the channel segmentation map or seasonal patterns. PG-87 is therefore generally stationary at the inlet throat.

North of the inlet in region 4 there is a SE migration pattern visible belonging to PG-87, starting in autumn of 2016. This pattern is part of the shoal bypass events caused by the "waggling" of the tail of PG-87, as described in Section 5.2. The SE directed velocity is on average 120 m yr^{-1}, though it has been accelerating in recent years. With this pace it will take roughly 7 years for the tail of PG-87 to be located just off the shore of the present location of the Rif. Therefore, at the end of the 2020's we can expect another shoal bypass.

The changes in the backbarrier basin of PG-87 can be traced in great detail. From the optical centerline map we know that the eastern channel of the eastern backbarrier branch of PG-87 (with this branch named PG-87E) has been stationary since 2013. In the SAR centerline map (region 5 in Figure 17) it has steadily drifted 74 m ENE (∼15 m yr^{-1}). The newer, western channel of PG-87E has different migration speeds along the channel. Its northern section rotated clockwise by 320 m in 4 years (80 m yr^{-1}) and will likely overtake the eastern channel. The central part of the western channel migrated 120 m ESE in the same years (30 m yr^{-1}).

The meandering of PG-87W (region 6) is going at a slow pace of 20 m yr^{-1}. The backbarrier channel of PG-00 in region 7 has migrated SE between the winters of 2016 and 2019 with an average velocity of 93 m yr^{-1}. This is the highest migration velocity of a backbarrier channel observed in both the green band and SAR centerline maps.

6 Conclusion

The goal of this work is twofold: 1) assess the existing conceptual models for the cyclic nature of the Pinkegat and the Engelsmanplaat by De Haan et al. (1983) and Oost (1995) respectively and 2) test novel remote sensing techniques for aiding in tracking changes in barrier island coastal systems. The conclusions of these two main research topics are therefore presented in two separate sections. The former topic also covers the impact of sand nourishments on the morphodynamic system.

6.1 Cyclic Nature of the Pinkegat and Engelsmanplaat

Pinkegat Throughout the time period spanned by the optical satellite imagery no single channel in the Pinkegat inlet became dominant. In 2019 the configuration of the channels was nearly identical to that at the start of the image sequence in 2000. Based on the starting year of the current cycle (∼1987) and the cycle period from the literature, another single inlet phase should occur in 2027 - 2037.

The channel PG-00 is thought to eventually form the single channel inlet. However, a merger with the easternmost channel PG-87 will take at least 30 yr, extending the current cycle into the 2040's. PG-87 lost a significant part of its basin in the west since 2010. This has changed its eastward migration into a slow westward one. Further changes in the basin could speed up its westward migration, thus shortening the time to a merger with PG-00 and thus a single inlet phase to the 2030's. The current cycle will however take longer than the expected 40 - 50 yr. We therefore argue that there is no cycle but a pattern of channel migration in the Pinkegat. These channels follow certain "behaviour rules" but are not on a fixed time schedule.

There are several details in the conceptual model by Oost (1995) which were tested. First of all, new channels were thought to form from spill-overs over the sandy shoal that forms the eastern end of Ameland. This is however observed to not be the case; instead, they form from the flood chute just off the coast. Smaller channels were observed to indeed migrate faster than the larger channels. Channel migration occurred at five times higher velocities in the winter compared to the summer periods. This indicates that the movement of the channels is mainly dictated by the waves, with the tides acting to maintain the total hydrodynamical balance in the system by for example maintaining the channel cross-section. The inlet has widened not only because of channel formation in the west, but also due to the migration of the Rif in the east.

Two other conclusions regarding the cyclic nature could be drawn. First of all, PG-87 reversed its curvature direction. This enabled a "wagging of the tail" type of behaviour of the channel in the ebb-tidal delta, creating a pattern of shoal bypassing events. The next will occur in 7 - 10 yr. Secondly, a tentative pattern of channel abandonment in the center of the inlet was observed. The previous channel that migrated this far east got abandoned in ∼2008. The channel PG-00 currently lies at roughly the same position and its recent major merger might induce another abandonment event. A revisit in roughly 5 yr will be needed to (dis)prove this theory.

Regarding the impact of sand nourishments updrift from the Pinkegat at Ameland, only a single event stood out: the channel PG-09 migrated at an extremely high velocity around 2016. This coincided with a major foreshore sand nourishment at Ameland in 2015. The channel migrated at a much lower rate before this nourishment. Other channels did not experience this boost in the same period however. A likely explanation is the fact that PG-09 was the only major and most westerly channel facing updrift. Any sediments from the nourishments would travel downdrift, enter the channel and be deposited in-place. This would speed up its migration while there is no additional sediment available for the other channels. Other causes for the quick migration can as of yet not be excluded. A detailed bathymetric study just before and during several years after a large nourishment is needed to accurately determine the impact in sediment transport and deposition.

Engelsmanplaat & Rif Though much of the erosion of the Engelsmanplaat occurred in the 1970's and 80's, it is still ongoing. Its supratidal surface area has more than halved between 2000 and 2019. Although predicted by Oost (1995), no further significant erosion at the western side of the Engelsmanplaat has occurred. The Rif is already in the same state as the Engelsmanplaat at its peak around 1970: hosting large complexes of embryonal dunes and having a peak height of around 2 m above mean sea level. Furthermore, the morphology of the islet is very similar to that of the Engelsmanplaat in the 1970's. Therefore, instead of merging with the Engelsmanplaat and resulting in the growth of the latter, the Rif has grown on its own to become a new Engelsmanplaat-type islet. This is supported by the fact that the Rif has not migrated south between 2000 and 2019 and is is undergoing erosion at its NW side. If this erosion rate will persist and will cause an equally fast migration of the shoal to the SE, it would take another 20 yr for the shoal to merge with the Engelsmanplaat. This results in a cycle which is 20% longer than expected. We therefore conclude that the cycle of the Engelsmanplaat has been altered. The cause of this seems to be the large transport of sand from the ebb-tidal delta of the Zoutkamperlaag to the shore of the Rif due to the closure of the Lauwerszee. This "sand boost" was of such a scale that the Rif could start growing through aeolian processes, halting the southward migration.

The Rif has underwent one shoal merger in the period 2000 - 2019, with another expected to occur within 2 years. The current configuration of channels in the Pinkegat is favourable for more of these sediment bypasses at a frequency of roughly once every 10 years. These enhance the growth of the Rif even further, solidifying its status as the "new" Engelsmanplaat. These sediment bypasses notably change the morphology of the Rif from a kidney shape to an arrowhead shape when the bypassed shoal is just offshore of the Rif. Wave refraction is the most likely culprit.

6.2 Remote Sensing Techniques

Two types of remote sensing data were used: optical and radar imagery. The former was available for a longer period but with a lower imaging cadence. The radar imagery on the other hand had a high imaging cadence but a lower total period in which data was available. This enabled these datasets to augment each other. The optical data traced the long-term

morphological change and mean migration velocities, while the radar data tracked changes throughout the seasons. Both datasets have a much higher cadence than the vaklodingen, enabling us to track individual channels and shoals in their evolution. The theory about the formation of new channels in the Pinkegat could therefore be tested. The data warranted the use of advanced image processing techniques. For example, wave induced backscatter in the radar imagery causes a lower contrast between water and land, which could be filtered using texture information (entropy). Other problems still need to be properly resolved, e.g. how to handle the low and high backscatter of land in radar imagery in comparison to medium backscatter for water, causing large networks of falsely detected channels.

With the second Sentinel-2 satellite in orbit since 2017, a much higher optical image cadence can be achieved. With the advantage of being able to look below the water surface, optical data will probably see more use than radar. However, the constant high frequency imaging of Sentinel-1 will still have a place in tracking morphological change. Techniques such as satellite derived bathymetry and radar interferometry, which are currently in development for coastal monitoring, will allow tracking sedimentary volume changes. This will open a completely new domain of coastal remote sensing and drastically improve tracking of morphodynamics in these regions.

References

Evert Attema, Pierre Bargellini, Peter Edwards, Guido Levrini, Svein Lokas, Ludwig Moeller, Betlem Rosich-Tell, Patrizia Secchi, Ramon Torres, Malcolm Davidson, and Paul Snoeij. Sentinel-1 - the radar mission for GMES operational land and sea services. *ESA Bulletin*, 131:10–17, Aug 2007.

CBS, PBL, RIVM, and WUR. Zeespiegelstijging langs de nederlandse kust en mondiaal, 1890-2017. 2018. URL www.clo.nl. indicator 0229, versie 10.

Commissie Monitoring Bodemdaling Ameland. Samenvatting monitoring effecten van bodemdaling op oost-ameland. 2017.

H. De Haan, R. IJbema, and D.T. Reitsma. *Engelsmanplaat: geschiedenis van en gebeurtenissen rond een zandbank.* Moddergat: Stichting 't Fiskershúske, Necumdruk, Drachten, 1983.

A. de Kruif. Bodemdieptegegevens van het nederlandse kustsysteem. beschikbare digitale data en een overzicht van aanvullende analoge data. 2001.

Job De Vries, Henk W. Van der Veer, and Elisabeth A. Addink. Object-based remote sensing van benthische macrofauna in de waddenzee. Technical Report 2, Waddenacademie, 2019.

Duncan M Fitzgerald, Shea Penland, and DAG Nummedal. Control of barrier island shape by inlet sediment bypassing: East frisian islands, west germany. *Marine Geology*, 60(1-4):355–376, 1984.

Edith L Gallagher, Steve Elgar, and RT Guza. Observations of sand bar evolution on a natural beach. *Journal of Geophysical Research: Oceans*, 103(C2):3203–3215, 1998.

Noel Gorelick, Matt Hancher, Mike Dixon, Simon Ilyushchenko, David Thau, and Rebecca Moore. Google earth engine: Planetary-scale geospatial analysis for everyone. *Remote Sensing of Environment*, 2017. doi: 10.1016/j.rse.2017.06.031. URL https://doi.org/10.1016/j.rse.2017.06.031.

SWE Huijs and JJP Lambeek. Geulmigratie op de buitendelta. *Het Friesche Zeegat en het Amelander Gat. Rapport R93-1, Instituut voor Marien en Atmosferisch onderzoek Utrecht (IMAU), Utrecht University, Utrecht*, 1993.

J.S. Lee. A simple speckle smoothing algorithm for synthetic aperture radar images. *IEEE Transactions on Systems, Man, and Cybernetics*, 13: 85–89, 1983.

Sonja Maria van Leeuwen. *Tidal inlet systems: bottom pattern formation and outer delta development.* PhD thesis, 2002.

Gerhard Masselink, Aart Kroon, and RGD Davidson-Arnott. Morphodynamics of intertidal bars in wave-dominated coastal settings—a review. *Geomorphology*, 73(1-2):33–49, 2006.

F.A.J. Minneboo. Jaarlijkse kustmetingen. richtlijnen voor de inwinning, bewerking en opslag van gegevens van jaarlijkse kustmetingen. 1995.

Saskia Mulder. Buitendijks erfgoed oostelijke waddenzee. 2015.

NAM. Report: Waddenzee – 1st lidar acquisition for 2018. Technical report, Nederlandse Aardolie Maatschappij B. V., 7 2018.

Albert Peter Oost. *Dynamics and sedimentary developments of the Dutch Wadden Sea with a special emphasis on the Frisian Inlet: a study of the barrier islands, ebb-tidal deltas, inlets and drainage basins.* Faculteit Aardwetenschappen, 1995.

AP Oost and H De Haas. The frisian inlet, morphological and sedimentological changes in the period 1970-1987. utrecht univ., inst. *Earth Sciences, Coastal Genesis Report*, 1992.

Fang Qiu, Judith Berglund, John R Jensen, Pathik Thakkar, and Dianwei Ren. Speckle noise reduction in sar imagery using a local adaptive median filter. *GIScience & Remote Sensing*, 41(3):244–266, 2004.

BG Ruessink, L Pape, and IL Turner. Daily to interannual cross-shore sandbar migration: Observations from a multiple sandbar system. *Continental Shelf Research*, 29(14):1663–1677, 2009.

LP Sha. Geological research in the ebb-tidal delta of 'het friesche zeegat'. *Utrecht The*

Netherlands.(RGD-Project 40010), 1992. URL http://publicaties.minienm.nl/documenten/geological-research-in-the-ebb-tidal-delta-of-het-friesche-zeegat-the-netherlands.

Stichting Verdronken Geschiedenis. Archief stichting verdronken geschiedenis. https://www.verdronkengeschiedenis.nl/nl/archief/archief.html, 2010. Accessed: 2020-01-13.

CT Swift. Passive microwave remote sensing of the ocean—a review. *Boundary-Layer Meteorology*, 18(1):25–54, 1980.

D Van der Wal and PMJ Herman. Quantifying the particle size of intertidal sediments with satellite remote sensing in the visible light, thermal infrared and microwave spectral domain. In *Proceedings of the ISPRS Commission VII Symposium 'Remote Sensing: From Pixels to Processes*, 2006.

D. Van Sijp. Correcties op gemeeten eb en vloed volume bij de omrekening naar gemiddeld getild in het friesche zeegat. *Notitie ANW 89-02.*, 1989.

Johan Van Veen. Onderzoekingen in de hoofden in verband met de gesteldheid der nederlandsche kust. *PhD thesis-universiteit van Leiden*, 1936.

Johan Van Veen. Eb-en vloedschaarsystemen in de nederlandse getijwateren. *Tijdschrift Koninklijk Nederlands Aardrijkskundig Genootschap*, 67:303–325, 1950.

Zheng Bing Wang. Morphodynamic modelling for a tidal inlet in the wadden sea:" het friesche zeegat". *Progress Report H0840*, 1991.

Zheng Bing Wang and Albert P Oost. Morphological development of the rif and the engelsmanplaat, an intertidal flat complex in the frisian inlet, dutch wadden sea. *Coastal Engineering Proceedings*, 1 (32):54, 2011.

N. Wiegmann. Onderzoek naar efficiency verbetering kustlodingen. 2002.

AM Winkelmolen and HJ Veenstra. Size and shape sorting in a dutch tidal inlet. *Sedimentology*, 21 (1):107–126, 1974.

Ivana Zinno, Manuela Bonano, Sabatino Buonanno, Francesco Casu, Claudio De Luca, Michele Manunta, Mariarosaria Manzo, and Riccardo Lanari. National scale surface deformation time series generation through advanced dinsar processing of sentinel-1 data within a cloud computing environment. *IEEE Transactions on Big Data*, 2018.

Appendices

A Figures

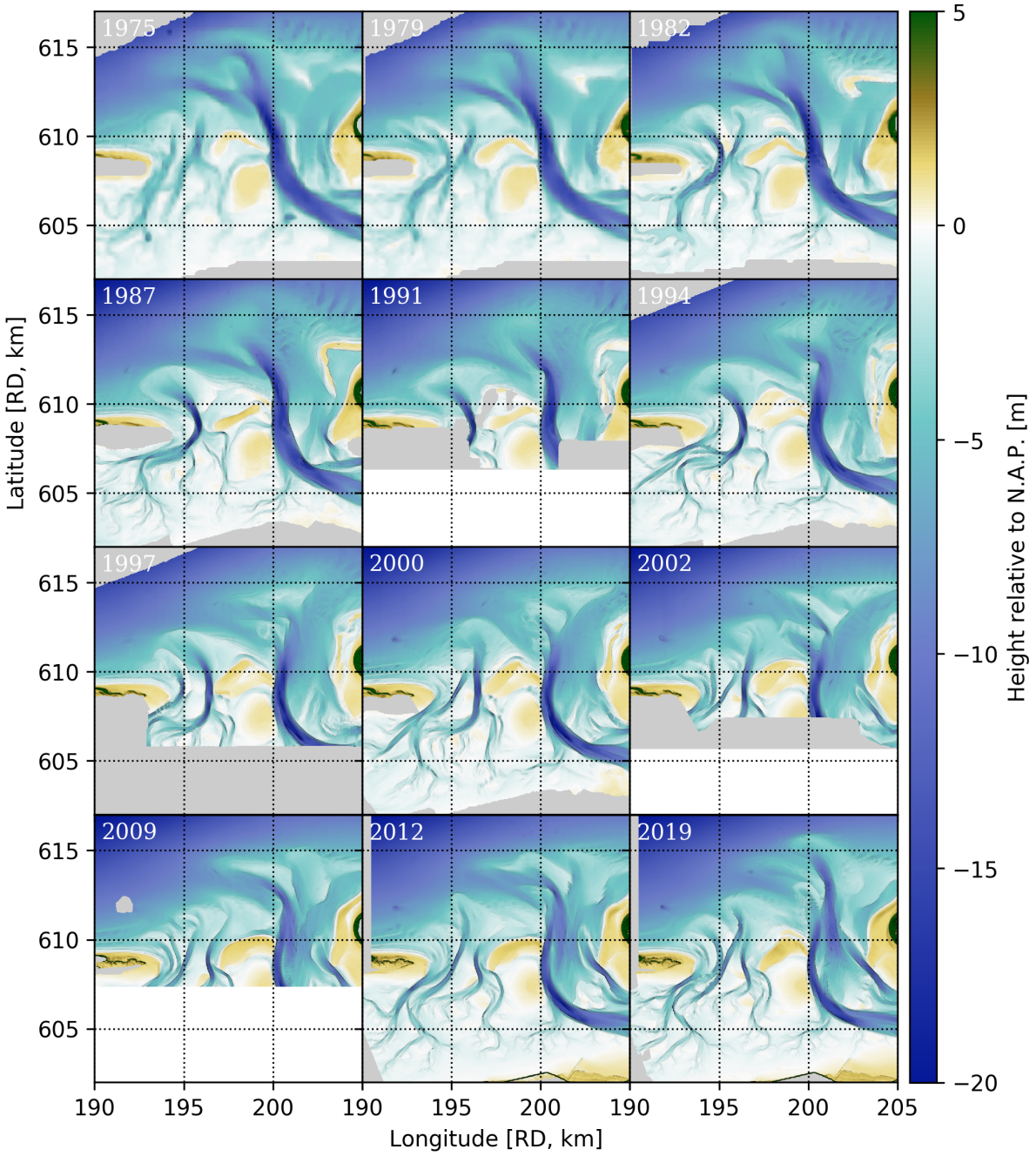

Figure 18: An overview of the available vaklodingen of the Frisian Inlet since 1975.

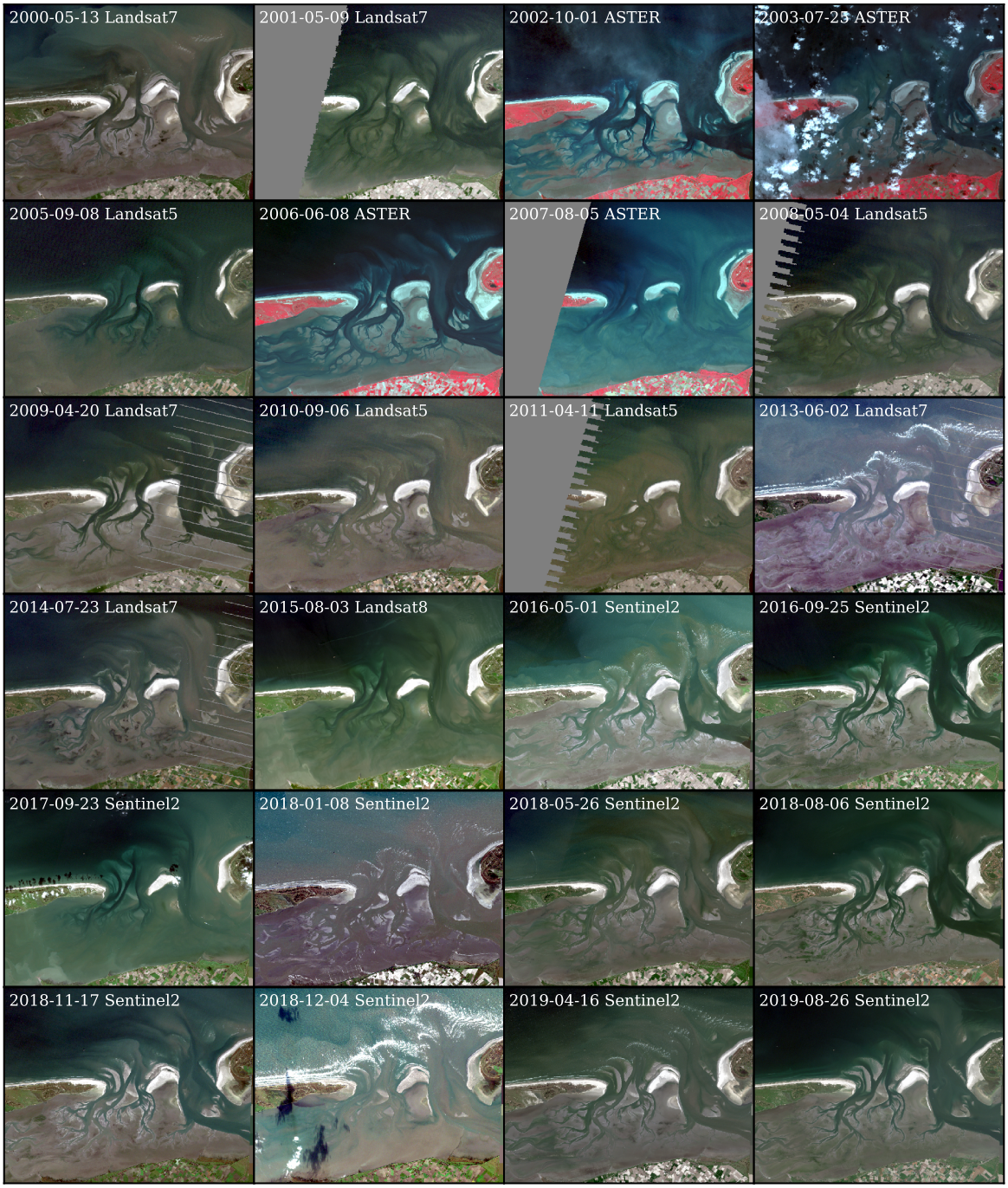

Figure 19: A series of RGB or NIR-RG images of the region of interest between 2000 and 2019. Note that in the years that Sentinel-2 data is available, more images per year are shown. This is done to showcase certain changes in the inlet occurring at short timescales like the erosion of a ridge separating two channels between 6-8-2018 and 17-11-2018.